21GRD08 SoMMet

D3: Report on the comparison and validation of existing neutron transport models used to interpret CRNS signals measured under outdoor conditions

Prepared by: UHEI, CMI, SMU, PTB, ASNR, PoliMi, UFZ, UNIBO, CNR, UP DE, TUBITAK and DTI

Organisation name of the lead participant for the deliverable: UP DE

Due date of the deliverable: December 2024

Actual submission date of the deliverable: 30 November 2025

Confidentiality Status: PU - Public, fully open

Deliverable Cover Sheet

Funded by the European Union. Views and opinions expressed are however those of the author(s) only and do not necessarily reflect those of the European Union or EURAMET. Neither the European Union nor the granting authority can be held responsible for them.

European Partnership Co-funded by the European Union

METROLOGY PARTNERSHIP EURAMET

The project has received funding from the European Partnership on Metrology, co-financed from the European Union's Horizon Europe Research and Innovation Programme and by the Participating States.

Deliverable **D3** of project 21GRD08 SoMMet

Report on the comparison and validation of existing neutron transport models used to interpret CRNS signals measured under outdoor conditions

Authors:
Markus Köhli (UHEI), Jannis Weimar (UHEI), Zdenek Vykydal (CMI), Jaroslav Šolc (CMI), Zuzana Pálková (CMI), Pavol Blahušiak (SMU), Jonas Marach (PTB), María de los Ángeles Millán-Callado (PTB), Miroslav Zboril (PTB), Ronan Lelièvre (ASNR), Nelson Magalotti (ASNR), Marco Caresana (PoliMi), Andrea Cirillo (PoliMi), Martin Schrön (UFZ), Peter Grosse (UFZ and UP DE), Gabriele Baroni (UNIBO), Anna Balenzano (CNR), Sascha E. Oswald (UP DE), Elodie Marret-Sicard (UP DE), Humbet Nasibli (TUBITAK), Emil Andreasen Klahn (DTI) and Henrik Kjeldsen (DTI)

Institutions:
UHEI – University of Heidelberg, Germany
CMI – Czech Metrology Institute, Czech Republic
SMU – Slovenský metrologický ústav, Slovak Institute of Metrology, Slovakia
PTB – Physikalisch-Technische Bundesanstalt, the National Metrology Institute of Germany
ASNR – L'Autorité de sûreté nucléaire et de radioprotection, Nuclear Safety and Radiation Protection Authority in France, formerly IRSN
PoliMi – Politecnico di Milano, Polytechnic University of Milan, Italy
UFZ – Helmholtz-Centre for Environmental Research, Leipzig, Germany
UNIBO – University of Bologna, Italy
CNR – Consiglio Nazionale delle Ricerche, National Research Council of Italy, Institute for electromagnetic sensing of the environment (IREA)
UP DE – University of Potsdam, Germany
TUBITAK – Türkiye Bilimsel ve Teknolojik Araştırma Kurumu, the Scientific and Technological Research Council of Türkiye
DTI – Danish Technological Institute, Denmark

Glossary

ASNR: French Authority for Nuclear Safety and Radiation Protection

ATB: Leibniz Institute for Agricultural Engineering and Bioeconomy

AWI: Alfred Wegener Institute for Polar and Marine Research

BSS: Bonner Sphere Spectrometers

BWE: Biomass Water Equivalent

CMI: Czech Metrology Institute

Cfb: Temperate oceanic climate (Köppen–Geiger classification)

CIEMAT: Centro de Investigaciones Energéticas, Medioambientales y Tecnológicas

CNR: National Research Council (Italy)

CNR-IREA: Institute for Electromagnetic Sensing of the Environment, CNR

CRNS: Cosmic-Ray Neutron Sensing

CRS-1000: Helium-3 proportional counter CRNS system

CRS-2000/B: BF_3 proportional counter CRNS system

DTI: Danish Technological Institut

DWD: German Meteorological Service

ERBSS: Extended-range Bonner Sphere Spectrometer

ESA: European Space Agency

Finapp 3: Lithium-6 doped scintillator CRNS system

FDR: Frequency-Domain Reflectometry soil moisture sensor

GFZ: German Research Centre for Geosciences

GEANT4: GEometry ANd Tracking, general-purpose high-energy transport code

GATE: Geant4 Application for Tomographic Emission

HERMEIS: High Energy Range Multisphere Extended IRSN System

IDW: Inverse Distance Weighting

LoD: Loss on Drying

MAXED: Unfolding code for neutron spectra

MCNP: Monte Carlo N-Particle (transport code)

NMDB: Neutron Monitor Database

NEMUS: NEutron MUltisphere Spectrometer

NEMUS-UMW: SI-traceable environmental version of NEMUS (Umwelt) nDSM: Normalised Digital Surface Model

PE: Polyethylene

PTRAC: Particle Track Output (pseudo file in MCNP)

PTB: Physikalisch-Technische Bundesanstalt

SAR: Synthetic Aperture Radar

SiPM: Silicon Photomultiplier

SMU: Slovak Metrology Institute

S1: Boron-10 lined gaseous CRNS detector (StyX Neutronica)

SoMMet: Soil Moisture Metrology

TDR: Time Domain Reflectometry

TDT: Time Domain Transmission

TOPAS: Tool for Particle Simulation (Wrapper for GEANT4 for clinical applications)

TUBITAK: Scientific and Technological Research Council of Türkiye

UDO II: Underground laboratory facility of PTB

UNIBO: University of Bologna (Italy)

UP DE: University of Potsdam (Germany)

USDA: United States Department of Agriculture

URANOS: Ultra RApid Neutron-Only Simulation

UTS: Universal Transport Function

W-PIE: Wide Energy Detector for Direct Investigation of Neutron spectrum at Ground level for Precise moIsture Evaluation

SWE: Snow Water Equivalent

fLoD: flow-based Loss-on-Drying

TABLE OF CONTENTS

Summary

This document (deliverable D3) is the third of eight technical deliverables of the project 21GRD08 SoMMet (hereafter: SoMMet). The project has received funding from the European Partnership on Metrology, co-financed by the European Union's Horizon Europe Research and Innovation Programme and by the Participating States (Funder name: European Partnership on Metrology; Funder ID: 10.13039/100019599; Grant number: 21GRD08 SoMMet).

SoMMet stands for "Soil Moisture Metrology". Soil moisture is a key variable influencing agriculture, forestry, groundwater recharge, weather, climate and greenhouse gas emissions. Several soil moisture observation systems exist at multiple spatial scales, but their measurements need to be harmonised. The overall objective of SoMMet was to develop novel metrological tools and to establish a metrological foundation for soil moisture measurements across lateral scales from decimetres to kilometres, thereby supporting reliable, SI-traceable and harmonised soil moisture measurements across methods and communities.

At the point scale (approximately 10^{-1} m – 10^{1} m), novel temperature and humidity metrology standards for soil samples were developed to reliably characterise soil moisture sensors. At the intermediate scale (10^{2} m – 10^{3} m), the metrological basis of the cosmic-ray neutron sensing (CRNS) method was established under laboratory and outdoor conditions, while at the large scale (10^{3} m – 10^{4} m), satellite-based remote sensing techniques were used to derive soil moisture products. Dedicated comparison campaigns enabled the development of tools for cross-disciplinary harmonisation and data fusion approaches integrating multi-scale measurements to generate high-quality, temporally and spatially consistent soil moisture information for land surface applications.

This document summarises the main results achieved during the SoMMet project within Work Package 2 (*Development of validation practices for CRNS methodology in outdoor conditions*), specifically in Tasks 2.1 (*Selection and further enhancement of high-level test field sites*) and 2.2 (*Validation of existing neutron transport models used to interpret CRNS signals specific to the soil moisture measurand*).

Three high-level agricultural test sites (Marquardt, Bondeno and Foggia) were selected and characterised in detail in terms of climate, land use, soil properties and instrumentation. Extensive soil sampling campaigns were conducted around CRNS sensors, combined with gravimetric analysis and point-scale sensors, and linked to a metrological traceability chain established within the project.

In parallel, four commercial CRNS systems were first characterised in neutron metrology laboratories (in Work Package 1: *SI-traceable measurement of soil moisture on point to field scale*, Task 1.3: *Calibration procedures for neutron-measuring devices of CRNS methodology*), where their digital twin models were validated. Subsequently, their performance under outdoor conditions was analysed together with systematic effects. The CRNS neutron measurements were complemented by specialised neutron detection systems (Bonner Sphere Spectrometers, a few-channel neutron spectrometer and a CRNS rover), which provided reference neutron spectra and datasets needed for benchmarking.

Building on these measurements, detailed digital twin models of the three SoMMet sites were developed with the URANOS neutron transport code, using voxel-based geometries, soil and vegetation maps and intensive soil sampling data. URANOS simulations were used to study CRNS footprint and depth sensitivity, the impact of vegetation and biomass water equivalent, and to reproduce CRNS time series at Bondeno and Foggia, while at Marquardt they were benchmarked against measured neutron energy spectra to quantify uncertainties.

A central methodological outcome is the concept of a “virtual reference CRNS neutron field”, generated with URANOS for a range of soil moisture states and used as a common neutron source to compute device-specific responses of the different commercial CRNS probes with validated MCNP models. Finally, model-based conversion functions from CRNS neutron response to volumetric soil moisture were evaluated and compared with existing approaches. Overall, the activities support the CRNS community’s efforts towards a harmonised framework for interpreting CRNS signals and the resulting intermediate-scale soil moisture estimates.

1 Introduction

Cosmic-Ray Neutron Sensing (CRNS) is a non-invasive method for measuring soil moisture over relatively large areas by detecting fast neutrons produced by cosmic-ray interactions. Details of the principles of the method can be found in the literature [Zreda et al. (2008), Desilets et al. (2010), Andreasen et al. (2017), Bogena et al. (2022)]. The method relies on an inverse relationship: cosmic rays generate secondary neutrons [Ziegler (1996)] that are efficiently moderated by hydrogen atoms in soil water through elastic scattering, so higher soil moisture leads to lower neutron count rates at a detector positioned above ground. The detection systems typically consist of neutron absorbers such as helium-3, lithium or boron, surrounded by a polyethylene moderator (2-3 cm thick), with the associated electronics, telemetry module and power supply housed in weather-resistant enclosures.

The measurement footprint is dynamic and environment-dependent [Köhli et al. (2015), Schrön et al. (2017)]. Horizontally, the sensor integrates soil moisture over a radius of approximately 130-240 meters (5-15 hectares), with maximum sensitivity at distances of about 20-80 meters from the detector. Vertically, the sensing depth ranges from roughly 15-20 cm in wet soils to 70-80 cm in dry soils. This intermediate spatial scale bridges the gap between point measurements and satellite remote sensing.

To obtain accurate soil moisture estimates from CRNS data, corrections are applied for atmospheric pressure and water vapour, vegetation biomass, soil chemistry (lattice water, organic carbon, neutron-absorbing elements), cosmic-ray flux variations and topography. The sensor provides area-averaged measurements with an hourly to daily temporal resolution and is widely applied in agriculture, hydrology and climate science.

This document describes the high-level test sites instrumented within SoMMet, the various detector systems used to conduct dedicated neutron measurements, and the systematic simulations of neutron transport at these sites. Benchmarking of the URANOS simulation code is presented, and the concept of a “virtual reference CRNS neutron field” is introduced, which couples the CRNS models previously validated in neutron metrology laboratories with the URANOS-based model of the environment. This enables a harmonised comparison of different CRNS sensor types under comparable (idealised) conditions. Finally, conversion functions from the CRNS neutron response to volumetric soil moisture are investigated, providing practical tools for CRNS end users.

2 High-level test field sites in SoMMet

2.1 Overview of the sites

The candidate test field sites available to the SoMMet consortium were reviewed. The review was based on evaluation criteria such as area extent, land cover, land use type, climatic conditions, soil heterogeneity and the instruments already deployed at the site. Based on this review, three sites were selected as high-level test field sites: ATB Marquardt near Potsdam in Germany (hosting participant: UP DE), Bondeno in the Emilia-Romagna region in northern Italy (hosting participant: UNIBO) and Foggia in the Apulian Tavoliere in southern Italy (hosting participant: CNR). The three sites are described as follows:

Marquardt near Potsdam, Germany

The Potsdam Soil Moisture Observatory (PoSMO) is located in the northwest of Potsdam, northeastern Germany (52.465°N, 12.959°E), covering an inner area of approximately 0.7 km² at 40 m a.s.l., with a broader representative area of about 3.4 km^2 of mixed agricultural land use, excluding forests and settlements. The site features flat to gently sloping lowland terrain on predominantly periglacial sandy soils (68–91 % sand, 8–27 % silt, 0.6–4.4 % clay), with organic matter content ranging from 0.4–17.3 % and bulk density averaging 1.3 g cm^{-3} in the top 30 cm. Managed primarily by the University of Potsdam's Institute of Environmental Science and Geography, in collaboration with the Leibniz Institute for Agricultural Engineering and Bioeconomy (ATB) and other institutions such as GFZ Helmholtz Centre, the observatory operates under a temperate Cfb climate (Köppen-Geiger climate classification) with mean annual precipitation of 584 mm (1981–2010) and average temperature of 9.3°C, including occasional snow events (e.g., 6 cm depth for eight days in February 2025) and frozen conditions, as well as drought and heavy rainfall periods.

Land use consists of 20 agricultural plots under mostly rain-fed management, featuring cereals, maize, alfalfa, sunflower, rapeseed, meadows, orchards (cherry, apple, maroni), young poplars, potatoes, and spring wheat, with limited irrigation on some crops and orchards; agricultural practices include sowing, harvesting, and tillage, with no significant changes in bulk density observed post-harvest or tillage.

Instrumentation since mid-December 2023 includes 16 stationary cosmic-ray neutron sensors (CRNS) from various manufacturers (e.g., Hydroinnova, Quaesta Instruments, StyX Neutronica) detecting epithermal neutrons for root-zone soil moisture monitoring (15–60 cm depth, 150–200 m radius footprint), co-located with 32 TDT sensors (Trübner SMT100) at 5 and 15 cm depths for shallow measurements, 20 soil moisture profile stations (using PR2/4, PR2/6, ThetaProbe ML2x, TDR probes) at depths of 9–200 cm, two groundwater observation wells (depths 1.5–10 m), two weather stations (ATB instrumentation directly on site, and meteorological station of the German Meteorological Service DWD at 12 km distance). Operational since 2019, with full extent from 2023, PoSMO serves as a high-coverage reference for validating satellite remote sensing products.

Bondeno, Italy

The Bondeno site is located in the flat agricultural area of the Po River plain, close to the city of Ferrara, Italy (44.855103°N, 11.383767°E). The site is planted with a walnut orchard (*Juglans regia* L. cv. Chandler) extending over approximately 160 ha and managed by Società Agricola Agro Noce S.r.l. The soil has a silty clay loam texture, according to the USDA classification. The field is divided into irrigated sectors, each controlled by independent valves and equipped with a micro-sprinkler system. Sprinkler nozzles are suspended 1 m above the soil surface and positioned along polyethylene (PE) tubes at 5 m intervals. The PE tubes have a water flow capacity of 80 $m^3\ h^{-1}$, and each nozzle has a water flow capacity of 0.078 $m^3\ h^{-1}$. A CRNS probe manufactured by Finapp S.r.l. (Montegrotto Terme, Padova, Italy) was installed at Bondeno in August 2021 and is part of a long-term monitoring site operated by the Department of Agricultural and Food Sciences of the University of Bologna (Italy). Within the SoMMet project, the site was upgraded with point-scale soil moisture sensors (SMT100) installed across the site and at different soil depths. The site is easily accessible by car and represents a suitable location for field activities and remote-sensing intercomparisons.

Foggia, Italy

The Foggia farm site is located in the Apulian Tavoliere region of southern Italy (41.460°N, 15.501°E), covering approximately 3 km^2 of flat cropland with clay loam soil. Managed by the National Research Council's Institute for Electromagnetic Sensing of the Environment (CNR-IREA), the site is characterized by an arid steppe climate with 530 mm of mean annual precipitation and temperatures averaging 15.8°C, with snow and frozen soil conditions being rare. The agricultural land is primarily used for durum wheat cultivation in winter and irrigated tomato production in summer, with regular ploughing to depths of 15-40 cm. Since 2017, the site has been instrumented with 10 capacitance soil moisture sensors (Decagon 5TM and 10 HS) measuring at depths of 2.5, 10, 20, and 40 cm, along with a weather station, making it a valuable validation site for Earth observation missions including Sentinel-1, Sentinel-2, and PRISMA. The site has supported multiple ESA and EU research projects focused on SAR-based soil moisture retrieval and agricultural monitoring, with historical data accessible to users and the location easily reachable by car.

2.2 Soil sampling campaigns on the SoMMet sites

For the interpretation of neutron count rates and their changes measured with a CRNS system under outdoor conditions, and for their conversion into integral soil moisture information, reliable point-scale soil moisture information is needed. This is typically obtained from manual soil sampling around the CRNS sensor and subsequent gravimetric soil moisture analysis in the laboratory. Additional time-series information is provided by commercial point-scale sensors buried in the soil at different depths and at various distances from the CRNS location.

The project consortium developed a traceability scheme that describes how SI-traceability is transferred from primary metrology standards, through transfer standards, to commercial sensors measuring soil moisture at the point scale and to CRNS sensors assessing soil moisture at the field scale. The SI traceability scheme was developed based on discussions with expert communities dealing with soil moisture and with the SoMMet Stakeholder Committee, as well as on an online survey. More details can be found in SoMMet deliverable D1 "*Report on the calibration of soil moisture measurement devices using a primary method, based on evolved water vapour detection,* *and transfer standards, such as 'standardised' loss on drying (LoD) or fibre coupled spectrometers, to ensure SI-traceable point-scale soil moisture measurements with uncertainties of 5 % under laboratory conditions*".

For point-scale soil moisture sensors, the traceability chain falls within the domain of temperature and humidity metrology. Reference methods for soil water content determination were developed by project participants DTI, TUBITAK and CMI. DTI and CMI adapted their existing primary-level metrology standards for water content in materials specifically for soil samples. TUBITAK developed its primary-level metrology measurement standard based on evolved water vapour detection. The systems, including uncertainty budgets and calibration procedures, were characterised and validated using both mineral and organic soils. DTI developed a mobile transfer standard based on the flow-based Loss-on-Drying (fLoD) method and validated it against the primary standard using organic and inorganic soils.

Gravimetric soil moisture measurements at the three soil physics laboratories (UP DE, UNIBO and CNR) associated with the high-level project sites were validated using DTI's transfer standard for soil water content determination. The procedure was as follows:

- Each field laboratory collected pairs of soil samples that were, as far as possible, identical from up to ten locations within the test field. One sample was measured by the field laboratory, and the other was sent to DTI for measurement. In several cases, not just one but three samples were taken at a given location and shipped to DTI for repeated measurements with the transfer standard. This allowed the variability between replicates to be analysed and the natural variability of soil moisture in "identical" samples to be quantified.

- The samples intended for shipment to DTI were packed in sealed aluminium bags, frozen and dispatched in polystyrene boxes. This procedure was used to keep the samples cold during transport and thus minimise biological activity that could change the water content in a soil sample. Temperature indicators were shipped with the samples to track their heat exposure.

- Comparisons between the field laboratories and the DTI transfer standard were carried out bilaterally, meaning that each field laboratory was benchmarked against the DTI results, which were considered as the reference. Sampling variability was quantified and taken into account in the statistical analysis of the soil water content determination results.

The gravimetric results showed that all three field laboratories were consistent with the DTI reference. Detailed results are not disclosed here, as they will be made publicly available either in the form of a peer-reviewed open-access journal article or in a separate report submitted to a trusted repository such as Zenodo. Overall, the successful validation of the three field laboratories (UP DE, UNIBO and CNR) demonstrates the robustness of the measurement systems and their suitability for SI-traceable soil moisture measurements across the project field sites along the chain of traceability.

3 CRNS methodology under outdoor conditions

Cosmic-Ray Neutron Sensing [Zreda et al. (2008), Desilets et al. (2010)] measures the environmental soil water content non-invasively by relating the above-ground neutron flux in a specific energy range to an inferred soil moisture curve.

The neutron radiation that can be detected in the natural environment, for example 1 m above the Earth's surface, spans about 12 orders of magnitude in energy: high-energy neutrons produced by cosmic rays can reach up to about 10^4 MeV, while subsequent scattering processes generate neutrons with progressively lower energies down to so-called thermalised (or thermal) neutrons with energies as low as 10^{-8} MeV. A typical neutron energy distribution (often referred to as a neutron energy spectrum, or simply neutron spectrum) encountered in natural environments is illustrated in Figure 1. For effective monitoring of integral soil moisture, CRNS systems have a characteristic response [Köhli et al. (2018)] tuned to the so-called epithermal neutron range, which spans approximately from 10^{-7} MeV to 10^{-1} MeV.

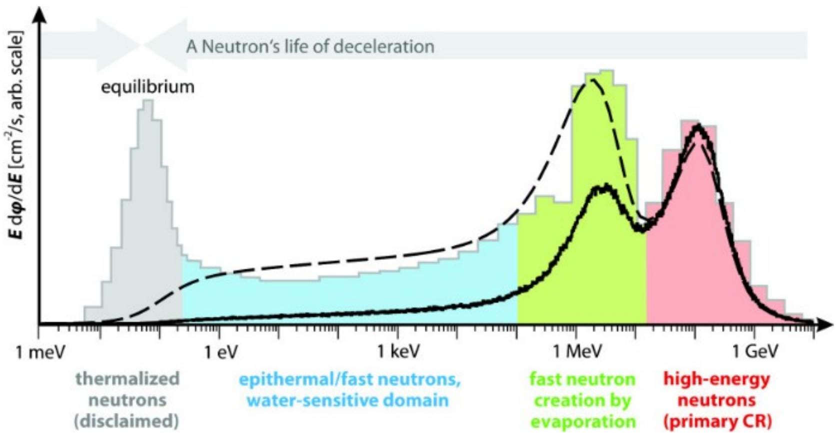

Figure 1. Neutron energy spectra at Earth's surface, adapted from Köhli et al. (2015). Colours illustrate the deceleration of initially high-energy neutrons (red), which interact with heavy atoms and produce an evaporation spectrum (green). Energy is then lost through elastic collisions with light atoms in the energy range to which a CRNS detector is particularly sensitive (blue), until the neutrons reach thermal equilibrium (light grey).

In this section, the specific types of CRNS sensors deployed in SoMMet are first introduced. Second, the main systematic effects that influence the CRNS methodology under outdoor conditions are summarised. Finally, the potential of environmental neutron measurements in specific settings is illustrated with selected examples.

3.1 CRNS sensors deployed in SoMMet

The following four types of commercial CRNS systems were used in the project. They are based on different neutron detection principles:

- Finapp 3 (Finapp S.r.l.) – lithium-6-doped scintillator [Gianessi et al. (2021)]
- S1 (StyX Neutronica GmbH) – boron-10-lined gaseous detector [Weimar et al. (2020)]

- CRS-1000 (Hydroinnova LLC) – helium-3 proportional counter [Zreda et al. (2012)]
- CRS-2000/B (Hydroinnova LLC) – boron trifluoride, BF_3, proportional counter

A separate document, deliverable D2 "*Report on the traceability scheme and uncertainty model for validation of neutron response functions of CRNS neutron measuring devices under laboratory conditions*", describes in detail the characterisation of these CRNS systems in neutron metrology laboratories. The main outcome of D2 is the development of digital twin models of these systems to support neutron transport calculations based on Monte Carlo simulation techniques, for example using the Monte Carlo radiation transport code MCNP [Goorley et al. (2012)].SoMMet, the CRNS digital twin models were validated through systematic experimental campaigns in the neutron reference fields of CIEMAT, CMI, PTB, SMU and ASNR. The CRNS systems were irradiated in well-defined, SI-traceable neutron fields to evaluate performance and investigate systematic effects under laboratory conditions. Based on the validated digital twin models, the response of the CRNS sensors to different neutron energy regions can be calculated. Figure 2 shows an exemplary result of the R&D activities summarised in deliverable D2. The CRNS systems have a characteristic response tuned to the so-called epithermal neutron energy range, which spans approximately from 10^{-7} MeV to 10^{-2} MeV. In this energy range, the CRNS methodology is effective as a monitoring tool for integral soil moisture.

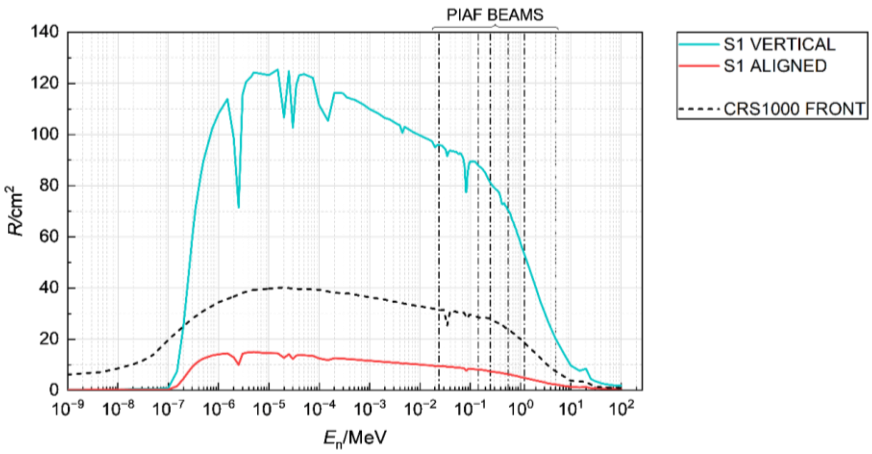

Figure 2. Characteristic response of a CRNS device to neutrons of different energies. CRNS systems are designed to predominantly detect neutrons in the epithermal neutron energy range, which spans approximately from 10^{-7} MeV to 10^{-2} MeV.

At the high-level test field sites introduced in Section 2, the following CRNS systems have been deployed for systematic data collection:

- **Marquardt near Potsdam:** At this site, a CRNS cluster consisting of 16 permanent, stationary CRNS systems of various manufacturers and types is operational. All four CRNS types listed above are deployed here.
- **Bondeno:** UNIBO operates one CRNS system of the Finapp 3 (Finapp S.r.l.) type.

- **Foggia:** CNR has operated one CRNS system of the CRS-1000 (Hydroinnova LLC) type since July 2024.

3.2 Brief review of systematic effects of CRNS

The following systematic effects, discussed in much more detail in the recent publication by Köhli (2025), must be considered when a CRNS system is deployed outdoors to monitor the dynamics of integral soil moisture [Köhli et al. (2020)] within the sensor footprint [Schrön et al. (2017)]:

A) Instrumental and software effects

Different detector types respond differently across neutron energy ranges, which can influence the characteristics of the soil moisture signal. Therefore, detector type and its neutron energy response must be taken into account to ensure consistent measurements. On-field calibration of CRNS instruments can also introduce uncertainties, particularly if relying on site-specific empirical relationships between neutron counts and soil moisture. Moreover, because CRNS is sensitive to both thermal and epithermal neutrons, shifts in sensitivity towards these energy ranges can lead to challenges in interpreting the measurements.

In addition, software version control becomes a key issue when a CRNS system is deployed for long-term soil moisture monitoring. CRNS systems run dedicated signal-processing software that distinguishes neutron events from other unwanted signals (e.g. electronic noise or signals from other particles). Any undocumented change in this software—for example in the neutron detection threshold settings or in the algorithms used to analyse electronic pulse shapes for selecting true neutron-induced events—can lead to different count rates that may mimic a change in soil moisture. This is particularly critical when the end user does not have access to the raw neutron signal time series.

B) Statistical and measurement uncertainty

The main challenge in operating CRNS instruments is the low natural cosmic-ray neutron flux, which drives statistical uncertainties, especially for short integration times (less than one hour). Typical precision is on the order of 3–5 % in volumetric soil moisture, although this depends on location, moisture conditions and atmospheric state. On-field calibration based on *in situ* field soil samples and empirical relationships introduces additional uncertainties, particularly at heterogeneous sites. Different assumptions about the neutron–moisture relationship and different calibration choices can lead to divergent results.

C) Environmental corrections and influences

Measurements with CRNS systems are influenced by a range of environmental factors. Air pressure is the most dominant factor, since neutron flux decreases with increasing pressure. Pressure also affects the measurement radius. At higher elevations, the effective range can be up to about 20 % larger than at sea level. Water vapor also influences the neutron count rate, so a humidity correction based on above-ground air humidity is required. The incoming cosmic radiation varies by site and geomagnetic configuration, which affects the primary neutron flux; this correction term is typically obtained from neutron monitors of the Neutron Monitor Database NMDB (www.nmdb.eu). Above-ground biomass (i.e. vegetation) tends to attenuate the CRNS signal because it can moderate neutrons. Corrections that account for plant height and density are applied, although their accuracy under different conditions is still under evaluation.

D) Soil and vegetation complexity

CRNS method is less sensitive to soil texture than many other methods, but uncertainties increase in highly heterogeneous soils. Vegetation dampens the neutron signal, so corrections based on plant height and density are necessary; however, the full influence of vegetation on neutron transport is not yet fully understood. Snow also affects the measurements. While correlations between snow water equivalent (SWE) and CRNS signals are generally promising, heterogeneous snow cover introduces additional uncertainties in interpretation which are not yet analytically understood.

E) Footprint and depth sensitivity

The CRNS footprint follows an approximately exponential pattern: areas closer to the sensor contribute more to the signal than more distant areas. Depending on moisture conditions, this footprint typically extends over a radius of roughly 130 to 220 m. Vertical sensitivity also decreases exponentially with depth, so deeper soil layers contribute less to the signal than near-surface layers. If soil moisture is inhomogeneous across the field, the resulting signal will deviate non-linearly, with drier areas exerting a disproportionately strong influence.

F) Simulation and modelling uncertainties

Monte Carlo simulation tools such as MCNP [Goorley et al. (2012)] and URANOS [Köhli et al. (2023)] are used to model neutron transport and to correct for environmental factors, but they inevitably simplify real field conditions. How accurately they represent actual geography and climate is critical for the validity of the results. Current CRNS footprint models often assume uniform soils, whereas real-world soils are heterogeneous and topography can be complex, which can reduce model accuracy.

3.3 CRNS and neutron measurements in specific environmental settings

In parallel with the systematic validation of the CRNS systems in neutron metrology laboratories, several CRNS sensors were also studied under specific outdoor conditions. CRNS sensors from the manufacturers Finapp and Quaesta Instruments were part of a comparison study on board the German research icebreaker RV Polarstern of the Alfred Wegener Institute for Polar and Marine Research (AWI). During the journey, the CRNS systems operated in a marine environment that is insensitive to soil moisture changes. At the same time, strong variations in the incoming cosmic-ray neutron energy spectrum occurred along the transect from Europe to the South Pole. This combination enabled an outdoor comparison of the CRNS systems. The survey is illustrated in Figure 3.

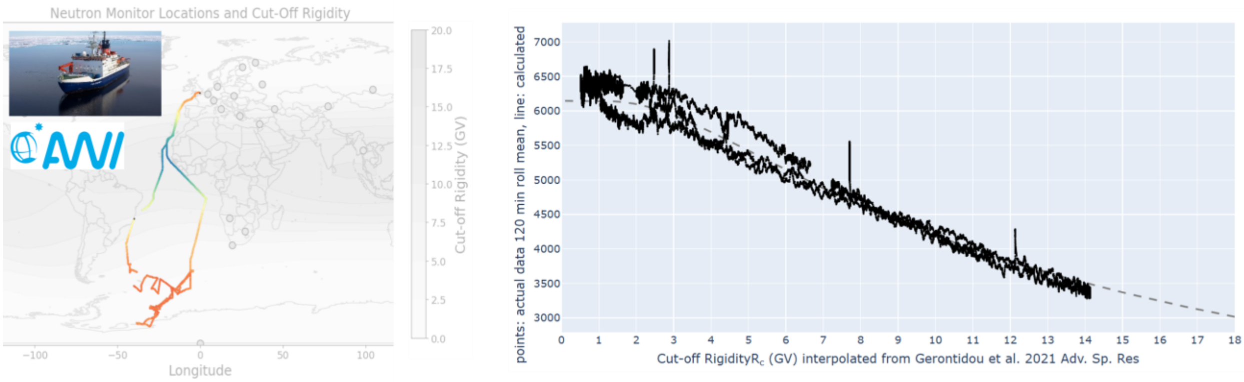

Figure 3. Latitude survey of neutron detector systems onboard the German research icebreaker RV Polarstern of the Alfred Wegener Institute for Polar and Marine Research (AWI). The experiment facilitated a comparison of CRNS detectors in terms of their sensitivity to different neutron energies along the changing Earth's magnetic field.

Another specific environment is the Ny-Ålesund Research Station on the Svalbard archipelago. Ny-Ålesund is the world's northernmost year-round research station, facilitating and hosting research projects and long-term observation series. The project participant UFZ operates there a Bonner Sphere Spectrometer (BSS) neutron detection system that can monitor neutrons of different energies and their response to environmental changes. Variations in near-surface water are much more extreme on Svalbard, while the geomagnetic cut-off rigidity is lower near the poles. There is potential for future comparison measurements between the BSS system at Ny-Ålesund and the mobile BSS system of the project participant PTB, introduced in Section 4. Such comparison measurements can, for example, provide insights into the effects of geomagnetic cut-off rigidity on cosmic-ray radiation. The system of UFZ is illustrated in Figure 4.

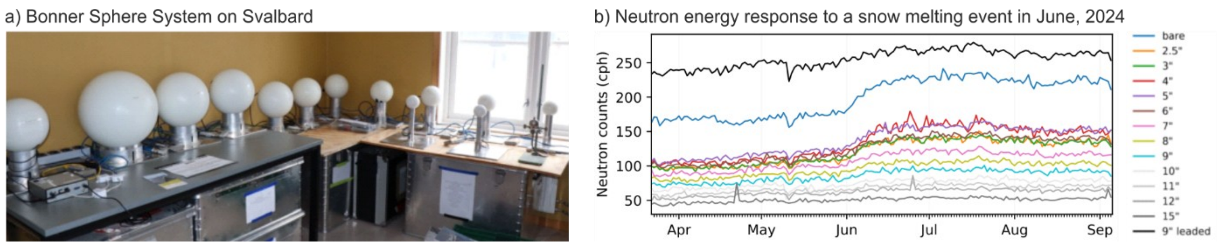

Figure 4. Neutron measurements with the Bonner sphere spectrometer system at the Ny-Ålesund Research Station on the Svalbard archipelago.

4 Overview of additional neutron detectors deployed in SoMMet

Here we briefly describe the neutron detection systems that were, in parallel to the commercial CRNS systems introduced in Section 3.1, used for measurements at the project sites described in Section 2. These additional systems were used to collect reference and supplementary datasets of environmental neutron radiation. These datasets were crucial for benchmarking the Monte Carlo-based neutron transport calculations, evaluating state-of-the-art approaches for correcting the incoming cosmic-ray neutron flux and quantifying the associated uncertainties.

As mentioned in Section 3, the energy spectrum of neutrons in the natural environment spans about 12 orders of magnitude, from about 10^4 MeV down to 10^{-8} MeV (see Figure 1). A widely used neutron spectrometric instrument capable of detecting neutrons across this wide energy range is the Bonner Sphere Spectrometer (BSS) [Bramblett et al. (1960)]. Its high-energy extension, the extended-range Bonner Sphere Spectrometer (ERBSS), extends this capability to higher neutron energies. An ERBSS system consists of a set of neutron-moderating spheres of different diameters and a thermal neutron detector placed at the centre of each sphere [Birattari et al. (2001)]. A typical set includes standard spheres made of polyethylene ($(C_2H_4)_n$) plus a few modified spheres with metal shells embedded in the polyethylene. Each sphere–detector combination has a different energy response to neutrons. For the standard spheres, the peak of the response function shifts to higher neutron energies as the size of the moderator is increased. For the modified spheres, the response increases significantly for neutron energies above approximately 50 MeV. In addition, it is common practice to perform measurements with the thermal neutron detector without a moderating sphere (i.e. the bare detector). Any combination of moderating sphere and thermal neutron detector is usually referred to as a "sphere", and this terminology is also applied to the bare detector. For historical reasons, sphere sizes are usually specified by their diameter in inches. Further details on neutron spectrometry with BSS can be found e.g. in [Thomas et al. (2002)].

4.1 Extended-range Bonner Sphere Spectrometer HERMEIS of ASNR

The ERBSS HERMEIS (High Energy Range Multisphere Extended IRSN System) instrument of ASNR (previously IRSN) [Cheminet et al. (2012)] consists of ten homogeneous polyethylene spheres with external diameters of 3, 3.5, 4, 4.5, 5, 6, 7, 8, 10 and 12 inches, as well as three additional spheres containing high-Z metal shells: 7- and 8-inch spheres with tungsten shells and a 9-inch sphere with a lead shell, referred to as 7"W, 8"W and 9"Pb, respectively. These high-Z converters are included to enhance the detection of high-energy neutrons via (n,*x*n) reactions. The thermal neutron detectors used inside are ^{3}He spherical proportional counters with a diameter of 5.08 cm (2 inch), filled with a partial pressure of 9.7 atm of ^{3}He and 0.3 atm of CO_2. The reaction of interest, ^{3}He(n,p)^{3}H, has a thermal neutron absorption cross section of 5330 barn, resulting in high detection sensitivity for moderated neutrons.

4.2 Extended-range Bonner Sphere Spectrometer NEMUS-UMW of PTB

PTB has been operating its ERBSS system, known as NEMUS (NEutron MUltisphere Spectrometer) [Wiegel et al. (2002)], for about two decades. For the SoMMet project, PTB developed an SI-traceable copy of the NEMUS system specifically for automated neutron spectrometry measurements under outdoor conditions. The new system, designated NEMUS-UMW (from the German *Umwelt*, meaning environment) consists of a new subset of NEMUS-derived Bonner spheres: six polyethylene spheres with diameters of 3, 4, 5, 6, 8 and 10 inches, a bare thermal neutron detector and four modified spheres with lead and copper shells.

The central thermal neutron detectors are spherical ^{3}He-filled proportional counters of type SP9, manufactured by Centronic Ltd. The specific SP9 counters used in the NEMUS-UMW system were selected for environmental neutron measurements—which are challenging due to the low levels of neutron radiation—because of their low intrinsic background. The intrinsic (instrumental) background of each SP9 counter was systematically tested and quantified in the "neutron-free" environment of the PTB underground laboratory UDO II [Neumaier et al. (2000)]. The electronics for neutron signal processing and telemetry in the NEMUS-UMW system comprise components that correspond to the state of the art in the CRNS community.

Using unfolding procedures, the neutron energy spectrum can be determined from the measured data and the spectrometer response functions. The response functions were characterised and validated in PTB's neutron reference fields, and both NEMUS and NEMUS-UMW serve as secondary metrological transfer standards for neutron fluence rate measurements. This means that the resulting unfolded neutron spectrum is determined in absolute terms, in units of neutron fluence $\Phi(E_n)$ in neutrons per cm^2. Figure 5 depicts the original NEMUS system of PTB, as well as the neutron response functions of the individual Bonner spheres in the system.

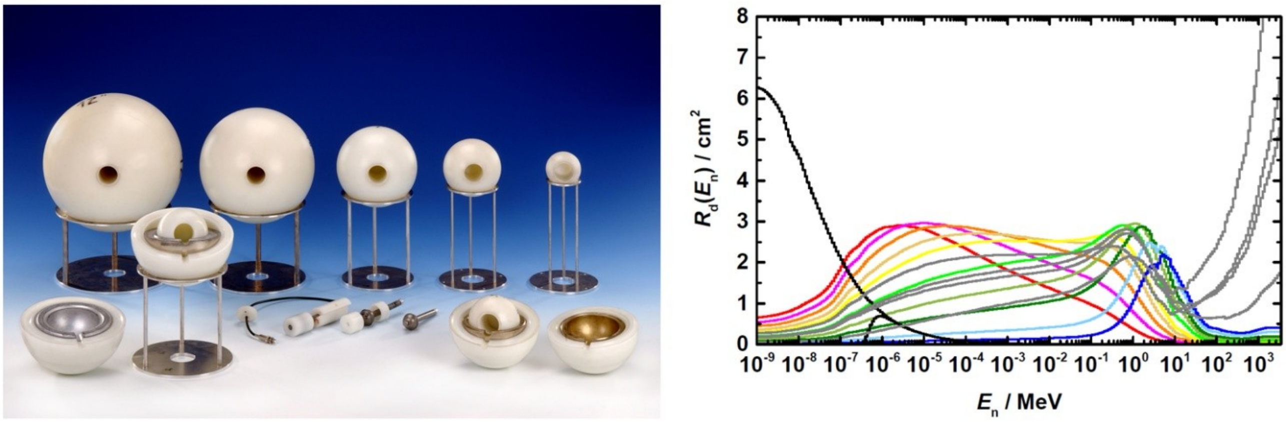

Figure 5. Setup of the PTB Bonner sphere spectrometer NEMUS (left) and the neutron response functions of the individual Bonner spheres (right). These response functions were validated in PTB's neutron reference fields and are therefore known in absolute units.

4.3 Few-channel neutron spectrometer W-PIE of PoliMi

Description of the system

The WEDDING-PIE (Wide Energy Detector for Direct Investigation of Neutron spectrum at Ground level for Precise moIsture Evaluation), abbreviated as W-PIE, is a neutron spectrometer developed by Politecnico di Milano. It is based on the thermal neutron counter M800, which consists of a ^{6}LiF converter inserted into a tube filled with ^{4}He. The tube is divided into eight segments that can be read out independently, making it equivalent to an ensemble of eight thermal neutron detectors.

The neutron detection mechanism is based on the reaction ^{6}Li(n,α)^{3}H. The reaction products deposit their energy in the helium gas, causing its excitation and subsequent de-excitation via the emission of scintillation photons. In each segment, three silicon photomultipliers (SiPMs) collect the scintillation light and generate the voltage signal corresponding to a neutron count. To reduce background to a negligible level, the acquisition system requires that at least two out of three SiPMs in a given segment detect a signal in coincidence for a neutron event to be registered. The schematic geometry of the M800 neutron counter is shown in Figure 6.

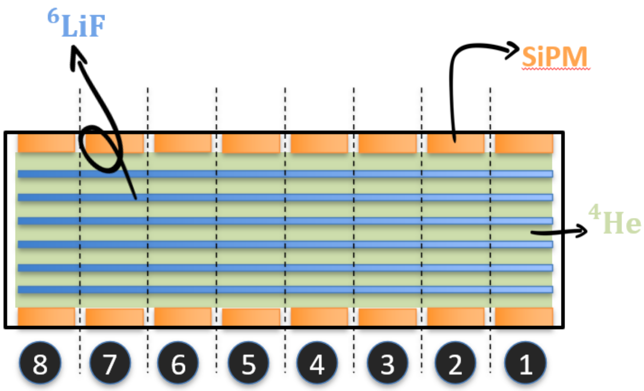

Figure 6. Simplified schematic of the geometry of the M800 thermal neutron counter used inside the W-PIE few-channel spectrometer.

In W-PIE [Cirillo et al. (2021)], the eight segments of the M800 counter are coupled in pairs, forming four independent sectors that are wrapped in different moderators. Specifically, the first sector is bare and is used to detect thermal neutrons; the second is covered by 2 cm of polyethylene and is mostly sensitive to epithermal neutrons; the third is covered by 7 cm of polyethylene and is sensitive to evaporation neutrons; and the fourth sector features a moderator made of polyethylene, lead and cadmium to enhance its sensitivity to high-energy neutrons. The overall geometry is illustrated in Figure 7.

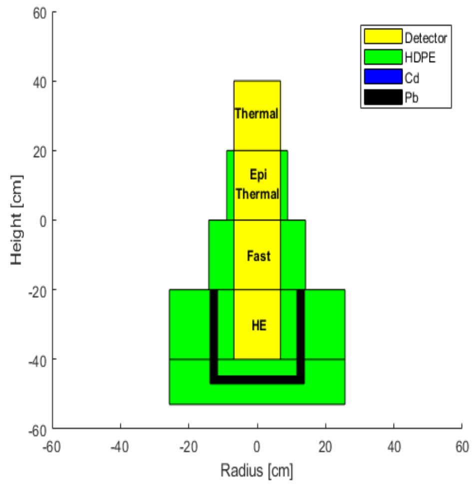

Figure 7. Schematised section of the W-PIE geometry.

Evaluation of the response functions

During a dedicated measurement campaign, the response of the detector was characterised with monoenergetic neutrons, which could be well approximated as an expanded and aligned field. However, this simplification cannot be applied to the cosmic-ray neutron field, whose angular distribution is complex and energy-dependent. The cylindrical shape of the W-PIE detector guarantees an approximately isotropic response in the radial direction, but not in the axial direction. For this reason, it was necessary to calculate the response of W-PIE for the specific double-differential energy–angle distribution of cosmic-ray neutrons. This was done using a two-step procedure:

1. A Monte Carlo simulation was first performed with MCNP to score the double-differential spectrum of cosmic-ray neutrons. The setup of the simulation is based on infinite horizontal layers, as depicted in in Figure 8. The source term is derived from EXPACS [Sato (2016)], a tool based on PHITS [Sato et al. (2015)]. In its most recent version, EXPACS provides particle spectra calculated excluding the Earth's albedo particles, which is a reasonable estimate of the incoming part of the neutron spectrum. The soil layer has a depth of 8 m and a bulk density of 1.43 g cm^{-3} with a porosity of 0.5. The solid components are SiO_2 (75 % by volume) and Al_2O_3 (25 % by volume), to which a volumetric water content of 20 % is added. Neutrons are scored in a spherical detector with a radius of 75 cm located 1.5 m above the ground.

2. The double-differential spectrum obtained in step 1 was then used to evaluate the response functions of the four sectors of the instrument in a second Monte Carlo simulation. The resulting neutron response functions are shown in Figure 9.

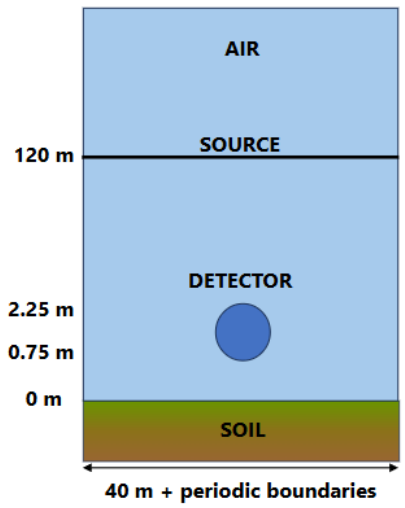

Figure 8. Setup of Monte Carlo simulations for assessing the cosmic-ray neutron energy and angular distributions relevant for the W-PIE system.

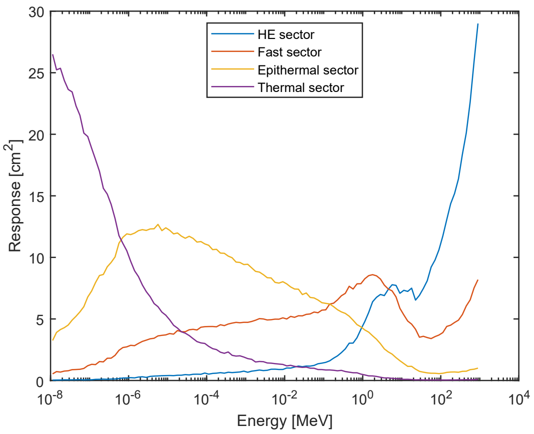

Figure 9. Evaluated response functions of the W-PIE system for detecting cosmic-ray neutron radiation.

The unfolding procedure is based on the GRAVEL algorithm [Reginatto et al. (2002)]. GRAVEL is an iterative spectral unfolding method that requires the user to provide a default spectrum. This default spectrum is adjusted iteration after iteration until a sufficiently low value of the χ^2 variable is reached, i.e. until a satisfactory agreement between the calculated solution and the measured data is obtained, given the statistical uncertainty. For the spectral unfolding, the uncertainty on the measured data is taken as the Poisson uncertainty of the counts, to which a relative standard deviation of 2.5 % is added. This additional contribution mainly accounts for the uncertainty associated with the response function calculation, which is affected by inaccuracies in the Monte Carlo model of the instrument and of the cosmic-ray neutron field.

Characterization of the W-PIE in field

During the measurements performed throughout the project, an unexpected behaviour of the M800 counter was observed when measuring natural radioactivity. The pulse-height distribution of events from neutron capture reactions is expected to preserve its shape in any neutron field. However, clear differences were found between the distributions observed for measurements of cosmic-ray neutrons and those obtained with an ^{241}Am-Be neutron source. This effect is shown in Figure 10: in field measurements, the detector records many more pulses with amplitudes higher than those caused by neutron captures.

It was assumed that this behaviour is due to contamination with Rn that may have occurred during the filling of the detector with ^{4}He. The long-lived progeny of ^{222}Rn have half-lives of up to about 22 years, thus providing an approximately constant background contribution to the neutron count rate. This contribution is negligible when measuring neutron fields with intensities higher than the environmental background but becomes relevant for the very low neutron fluxes encountered in natural environments.

To test this hypothesis, the M800 detector was placed in the PTB underground facility UDO II, which is located in a salt mine at a depth of about 400 m below ground. The overlying rock mass strongly attenuates incoming cosmic-ray–induced radiation, so in this case the count rate measured by the detector is expected to be dominated by its intrinsic background. The pulse-amplitude spectrum measured at UDO II is shown in Figure 11: as expected, the detector records many events with amplitudes greater than those corresponding to neutron capture events. The average measured count rate is approximately 1250 counts per hour (sum of all segments). This background signal must be subtracted from the on-field count rate to derive the true contribution of cosmic-ray neutrons.

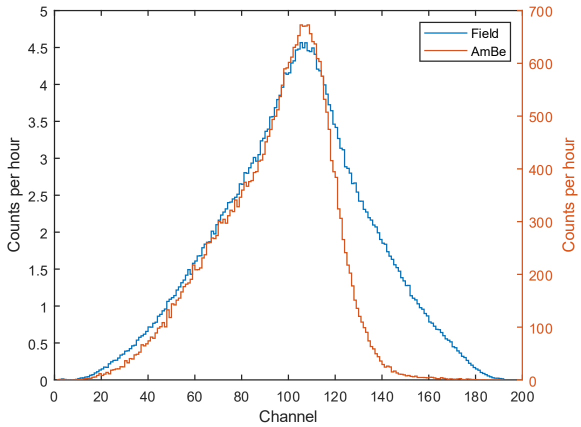

Figure 10. Comparison between the W-PIE pulse height distributions for a neutron source and for environmental neutron measurements.

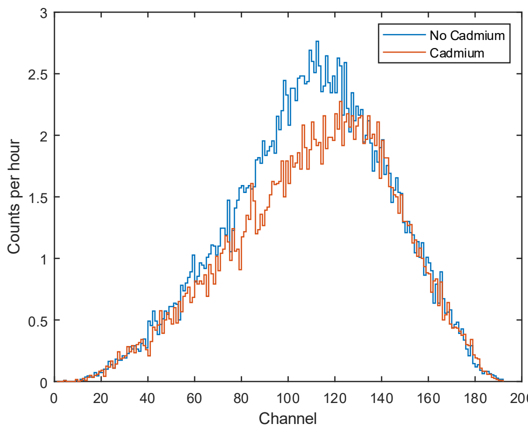

Figure 11. W-PIE pulse height distributions showing the intrinsic background signal as measured in the "neutron free" environment of the PTB underground laboratory UDO II.

4.4 CRNS Rover of UFZ

The CRNS rover of UFZ is a mobile application of the CRNS method for field-scale soil moisture mapping. The system consists of a vehicle-mounted moderated neutron detector with a GPS, meteorological sensors and data acquisition and telemetry units. This allows non-invasive surveys of root-zone soil moisture along transects or areas spanning from hundreds of metres to several kilometres. By continuously recording neutron count rates while the instrument is in motion, the rover provides spatially distributed soil moisture estimates as snapshots. Further details are available in the literature [Schrön et al. (2018)].

5 Selected results obtained with CRNS sensors and reference neutron detectors deployed in SoMMet

In this section, we describe selected results obtained at the SoMMet test field sites using commercial CRNS sensors, as well as specialised neutron detectors that provided reference and/or additional neutron datasets required for an improved understanding of the CRNS methodology.

5.1 ERBSS HERMEIS at the Bondeno site

Two measurement campaigns were conducted at the Bondeno site from 31 March to 5 April 2025, and from 10 to 14 June 2025. For logistical reasons, only the 3”, 4”, 5”, 7”, 8”, 10”, 7”W, 8”W and 9”Pb Bonner spheres were used. They were operated simultaneously and placed approximately 1.5 m above the ground and about 4 m away from a barn (see Figure 12).

Figure 12. Setup of the HERMEIS ERBSS system of ASNR as deployed for outdoor neutron spectrometric measurements at the Bondeno site.

During the first campaign, very unfavourable weather conditions (strong wind and rain) required positioning the tent and the spheres relatively close to the building to provide better shelter. Despite this precaution, the measured energy deposition spectra in the ^{3}He counters of each sphere were very noisy, leading to reduced measurement times, low counting statistics and statistical uncertainties exceeding 10 %. For this reason, a second measurement campaign was carried out using the same setup and configuration, but under much better weather conditions.

The measurements obtained during the second campaign therefore showed much better counting statistics (between 3000 and 7000 counts per sphere over the entire week) and exhibited significantly less noise. To observe the evolution of the neutron spectrum over time and verify the consistency of the results with potential changes in soil moisture, day-by-day analyses were first performed. For this purpose, corrections were applied to the daily count rates to isolate the effect of soil moisture and remove the influence of other factors (such as variations in atmospheric pressure and incoming neutron flux).

The daily neutron spectra, shown in Figure 13, were then obtained using the MAXED unfolding code [Reginatto et al. (2002)], with the guess spectrum (initial "default" spectrum) simulated by the URANOS code. These neutron spectra are very similar, especially in the epithermal energy range (i.e. the domain of interest), where fluence rates between 6.6 and 7.8 n cm^{-2} h^{-1} were measured, with a standard deviation of only 8 %. This nearly constant epithermal neutron fluence over time is consistent with the stable weather conditions observed during this measurement campaign and demonstrates- the robustness of the measurements.

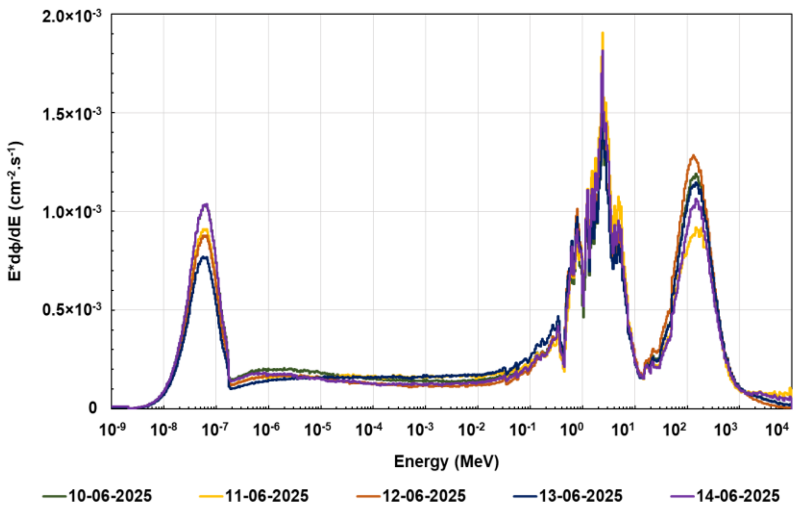

Figure 13. Day-by-day comparison of neutron spectra derived from HERMEIS measurements at the Bondeno site using the MAXED unfolding code.

The URANOS code was also used to simulate the neutron spectrum at the Bondeno site for different soil moisture values. Since the daily neutron spectra are very similar, the simulated spectra were compared with the neutron spectrum obtained by combining all count rates measured during the week-long campaign, thereby enhancing statistical quality and robustness (see Figure 14). Note that the simulated neutron spectra were scaled by an arbitrary factor to enable a qualitative comparison with the measured spectrum.

Figure 14 shows that URANOS correctly reproduces the overall spectral shape, particularly in the thermal-to-fast energy range, with somewhat larger discrepancies at higher energies. Nevertheless, URANOS proves to be well suited for simulating neutron interactions with soil moisture and predicting the resulting neutron spectrum, as the energy range of interest (the epithermal range) is accurately reproduced by the simulations. Thus, despite the technical challenges associated with outdoor measurements, robust and consistent results were obtained, providing reference neutron spectra suitable for benchmarking the URANOS code.

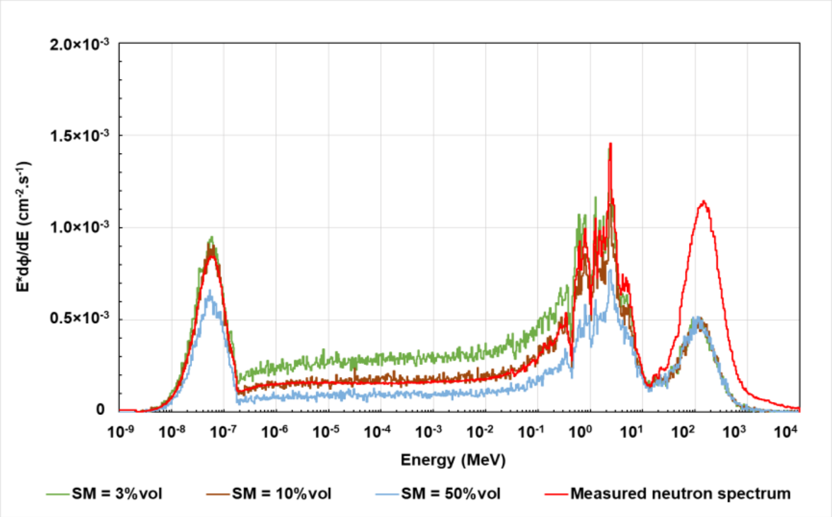

Figure 14. Comparison between the neutron spectrum derived from the full-week measurements with the ERBSS HERMEIS of ASNR and simulated neutron spectra predicted by the URANOS neutron transport code for different soil moisture values.

5.2 ERBSS NEMUS-UMW at the Marquardt site

On 18 June 2025, the NEMUS-UMW system of PTB was installed at the Marquardt site at a location with permanent power supply and at a distance of 9 m from CRNS station #31. Station #31 is part of the CRNS cluster that is operated long-term at the site by UP DE. The overall setup of NEMUS-UMW and its components is shown in Figure 15. In total, 11 neutron detectors placed in individual Bonner spheres are read out simultaneously in a synchronised manner. The system operates autonomously, and the data are sent via telemetry to the PTB server every 30 minutes.

The objective of this campaign is twofold: first, to obtain time series of neutron count rates for each spectrometer sphere; and second, to provide unfolded neutron spectra averaged over periods of several hours on different dates and times. As of September 2025, the NEMUS-UMW system had remained fully operational for more than three months of continuous data taking, despite challenging weather conditions such as heat waves, high relative humidity, heavy rainfall and storms. The measurement campaign is planned to end in December 2025. The datasets collected during the project and the resulting unfolded neutron spectra are discussed in Section 6.2.3, where they are used for benchmarking the URANOS simulation code.

Figure 15. Photographs of the individual components of the PTB Bonner sphere spectrometer NEMUS-UMW for environmental neutron measurements: (a) neutron detectors of type SP9 (Centronic Ltd.); (b) neutron detectors coupled to all-in-one electronic readout modules of type NPM (Neutron Pulse Monitor, Quaesta Instruments); (c) subset of polyethylene neutron-moderating spheres; (d) four "modified" spheres with lead or copper shells for detection of high-energy neutrons; (e) bare SP9 neutron detector and NPM module placed in a weatherproof casing; (f) SP9 detector placed inside an 8-inch sphere and NPM module placed in a weatherproof casing; (g) full setup as deployed at the Marquardt test field site, about 9 metres from CRNS station #31 (visible on the left side of panel (g)).

5.3 Few-channel neutron spectrometer W-PIE at the Bondeno site

W-PIE was installed at the Bondeno site during the periods 31 March–5 April and 10–16 June, in proximity to the HERMEIS spectrometer (the distance between the systems was approximately 15 m). In this configuration, it is reasonable to assume a sufficiently uniform cosmic-ray neutron fluence between the two devices and thus to perform a meaningful comparison between the spectra unfolded by the two systems. The following analysis focuses on the data collected in June, for which both systems acquired sufficiently robust measurements. The detector was placed on three wooden pallets, so that its base was 45 cm above the ground and its maximum height was approximately 1.5 m.

To obtain sufficient statistics for meaningful spectra, the neutron count rates were averaged over one-day observation periods. Figure 16 shows the average daily count rate of the four sectors during the observation period. The data are corrected for the intrinsic background of the instrument but do not account for changes in environmental parameters (air humidity, incoming neutron flux and air pressure). The average daily values of air humidity and pressure were monitored by a weather station (Vaisala WXT536) installed near the instrument. Fluctuations in the incoming neutron flux were estimated using data from the neutron monitor at the Jungfraujoch station. The corresponding correction factors are shown in Figure 17. The observation period was characterised by stable atmospheric conditions, and the fluctuations due to variations in environmental parameters were limited to ±2 %.

For each day, the neutron spectrum was unfolded. The default spectrum used in this case is the Monte Carlo simulation obtained with URANOS, identical to that used for the unfolding with the HERMEIS ERBSS. This means that both neutron spectrometers derived the neutron energy distribution starting from the same default spectrum and using the same unfolding code, GRAVEL. In this way, it is reasonable to assume that differences between the solutions are due to the measurements of the devices themselves, rather than to effects introduced during the subsequent data analysis.

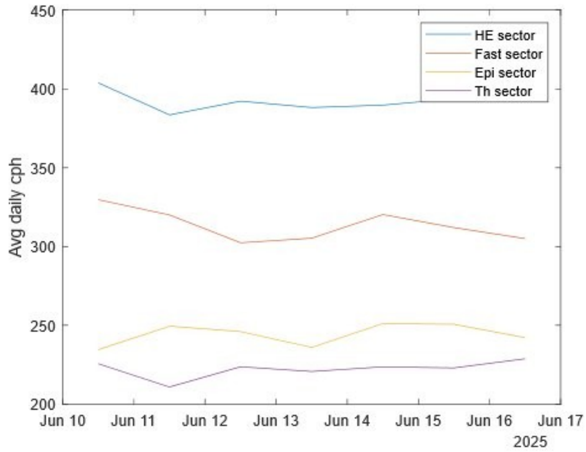

Figure 16. Average daily count rates measured with W-PIE in Bondeno.

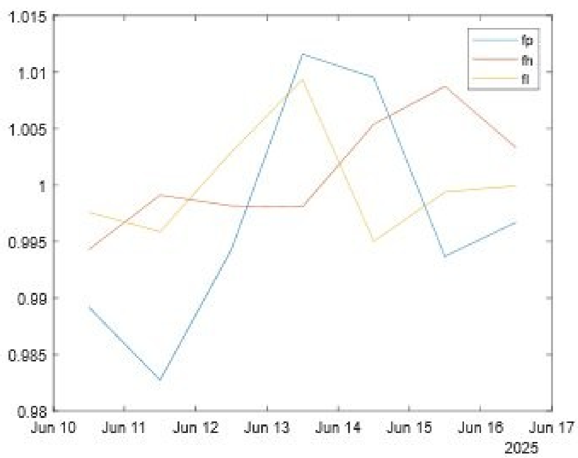

Figure 17. Correction factors for environmental parameters during the measurement period with W-PIE in Bondeno.

The unfolded average daily spectra are shown in Figure 18. As expected from the stable atmospheric conditions and the nearly constant count rates, the calculated neutron spectra do not exhibit any pronounced variations during the observation period. The most noticeable difference is observed for the spectrum of 10 June (the first day of measurement) compared with the other days. However, the spectrum for this day is based on poorer statistics, since the installation was completed in the early afternoon and the daily average is computed over only 8 hours of measurements instead of 24.

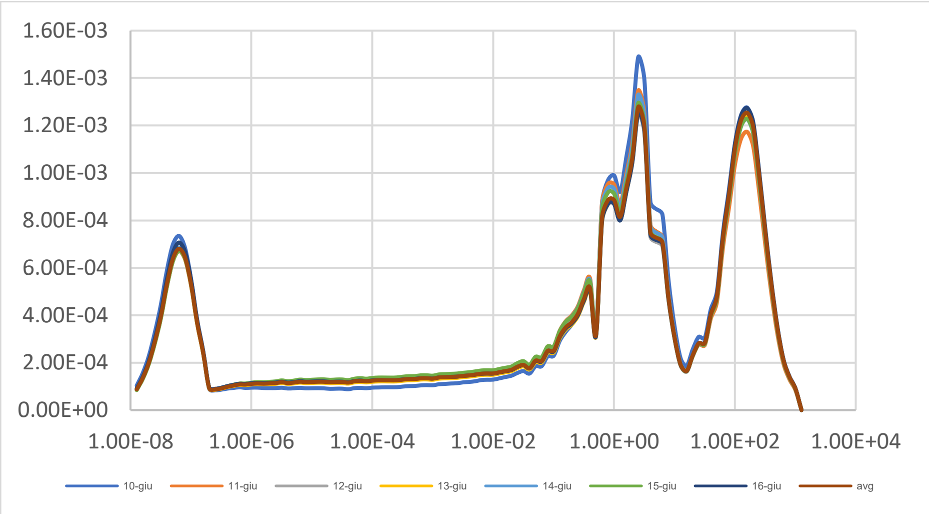

Figure 18. Unfolded neutron spectra from daily averaged neutron data collected during the W-PIE measurement campaign in Bondeno.

The neutron spectra unfolded with W-PIE and with the HERMEIS were then compared. For this comparison, weekly average count rates were used. Since W-PIE operated continuously, whereas the HERMEIS was only running for several hours per day, the W-PIE averages were computed considering only the periods during which both instruments were measuring simultaneously. The comparison is shown in Figure 19. The spectral resolution achievable with W-PIE is lower than that of the HERMEIS, mainly because W-PIE is based on four neutron detectors, whereas the ERBSS HERMEIS provides many more measurement channels. Good agreement is found for the evaporation and high-energy neutron ranges, while the agreement is poorer for the thermal and epithermal ranges.

Table 1 summarises the neutron fluence rates calculated by the two systems for different energy regions.

Table 1. Evaluated neutron fluence rates by the W-PIE and the BSS in different energy regions.

Neutron Energy Region	W-PIE [cm^-2h^-1]	BSS [cm^-2h^-1]
<0.5 eV	4.3	5.5
0.5 eV – 0.5 MeV	8.4	9.7
0.5 MeV – 10 MeV	9.0	8.6
> 10 MeV	9.6	9.84
Total	31.3	33.7

The W-PIE showed good agreement with the HERMEIS reference system in the energy regions above 0.1 MeV, whereas it underestimated the neutron fluence rate by about 13 % in the epithermal region and by about 20 % in the thermal region. This deviation would be acceptable for neutron dosimetry, where the main regions of interest are at higher energies. For CRNS, however, such an underestimation is more critical, as it affects the energy regions to which the detectors are most sensitive. This result suggests that the responses of the thermal and epithermal sectors of W-PIE are not perfectly modelled by the Monte Carlo code when simulating irradiation by the cosmic-ray neutron field. One possible reason for this discrepancy is the shape and dimensions of the detector itself: because the base of the instrument is wide and heavily moderated, it strongly attenuates the intensity of low-energy neutrons reaching the upper part of the detector, thereby reducing the count rate of the thermal sector. It is possible that the simplified Monte Carlo simulations used to evaluate the response functions do not represent this effect sufficiently well, thus overestimating the detector response to thermal neutrons and biasing the unfolding procedures.

W-PIE proved to be stable in operation during the measurements, with a generally simpler setup and less demanding logistical and power requirements compared to the ERBSS. Its measurements showed excellent agreement with the HERMEIS spectrometer for energies above 1 MeV, whereas some doubts remain regarding their accuracy in the thermal and epithermal energy regions. It would therefore be valuable in the future to conduct a longer intercomparison between W-PIE and an ERBSS system for environmental neutron measurements, in order to investigate the origin of this discrepancy in more detail and, if possible, resolve it.

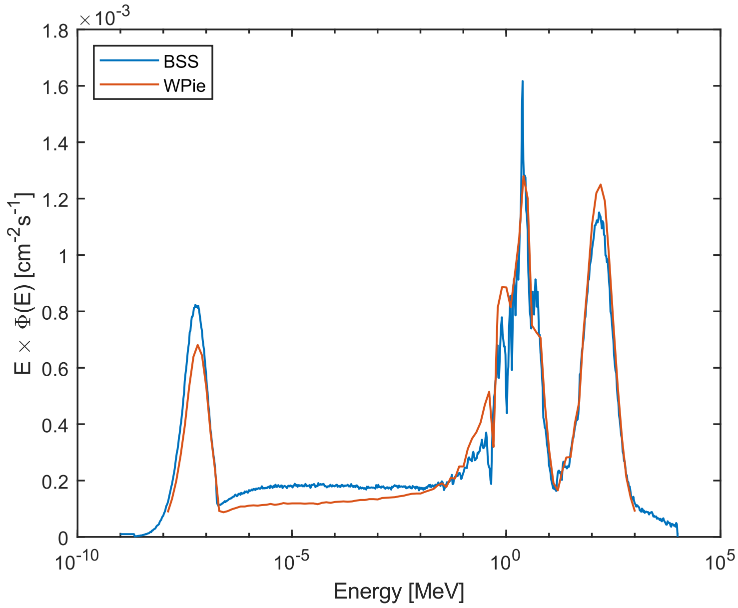

Figure 19. Comparison between unfolded neutron spectra obtained with the W-PIE and ERBSS HERMEIS neutron instruments at the SoMMet site Bondeno.

5.4 CRNS Rover at three SoMMet sites

Mobile CRNS measurements were performed at the three test sites Bondeno, Foggia and Marquardt. The detector type is a Hydroinnova ^{3}He-based system [Schrön et al., 2018] and is therefore comparable to the CRS-1000 detectors characterised in the laboratories. The vehicles used (handcart, car, forklift) are mainly made of metals and are thus largely transparent to neutrons. For direct comparison with point sensors, the detector was modified with 15 cm thick polyethylene shields at the sides and on the top to reduce the CRNS footprint to approximately 1 m^2. The resulting soil moisture maps were used for comparison with soil moisture derived from manual soil sampling campaigns and with measurements from commercial point-scale sensors buried in the soil. The roving campaigns also supported the generation of spatially distributed soil moisture information required as input for the URANOS simulation domains at each of the three SoMMet sites. Exemplary results obtained with the CRNS rover are illustrated in Figure 20.

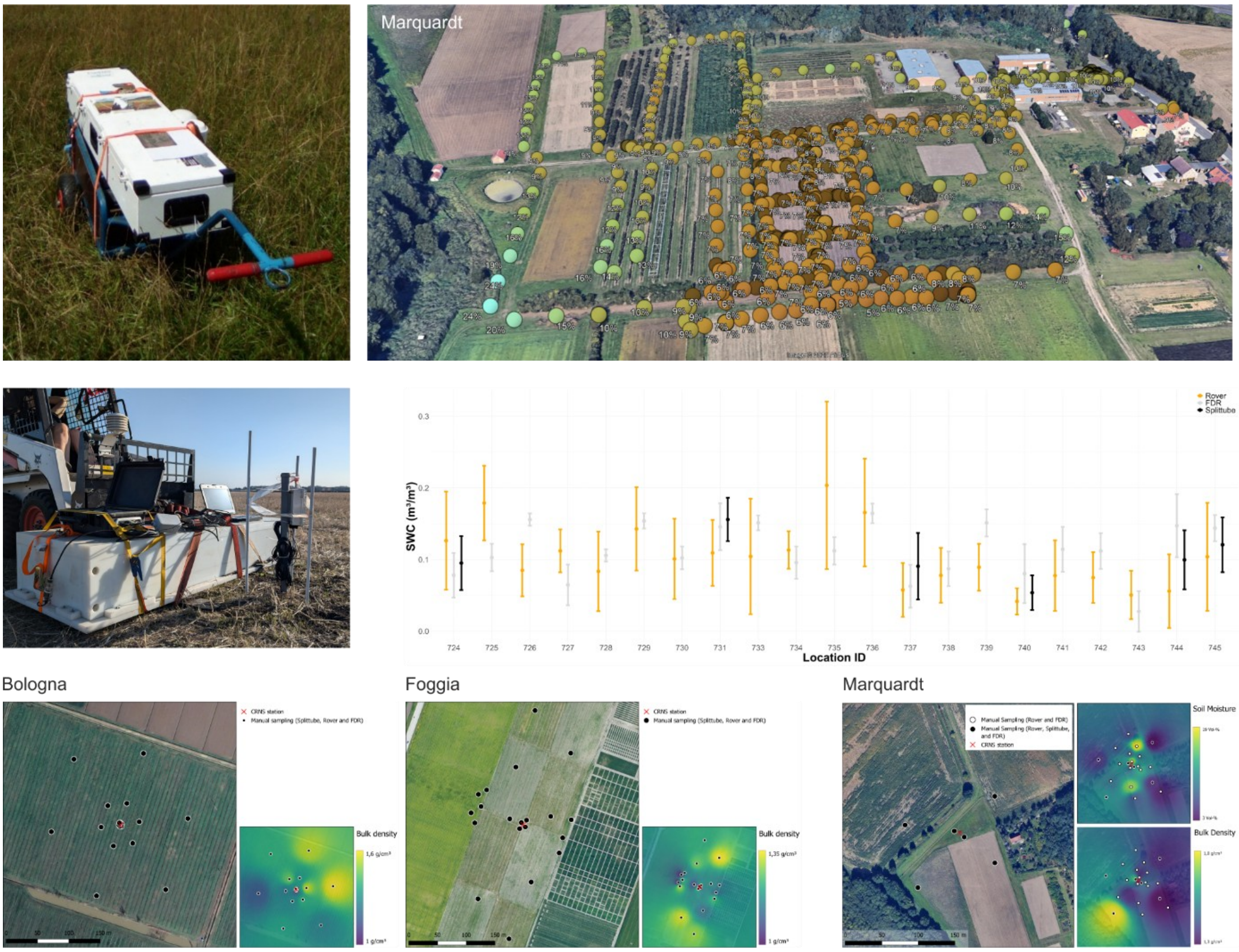

Figure 20. Mobile CRNS measurements at the three test sites to facilitate comparison with point-scale sensors and models. Top panel: mobile measurements by hand wagon in Marquardt. Mid panel: Shielding CRNS measurements in Bondeno and comparison with soil moisture from sampling and FDR (frequency-domain) point-scale sensors. Bottom panel: Measurement design and site heterogeneity in the stationary CRNS footprint at the three test sites.

6 Digital twin models of the SoMMet outdoor sites

In this section, we describe the generation of digital twin models for the three SoMMet outdoor sites. These models consider the individual topographical and environmental settings of each site and were subsequently used for systematic neutron transport simulations in which a range of environmental parameters was considered, one of the most important being soil moisture. This approach enables us to establish a link between soil moisture and the neutron fluence rate reaching a neutron detector (CRNS sensor) situated above ground.

6.1 Overview of neutron transport simulation codes

MCNP (Monte Carlo N-Particle) [Goorley et al. (2012)] was developed at Los Alamos as a general-purpose code to simulate neutrons, photons, electrons and their coupled transport. Versions up to MCNP4 were capable of simulating neutrons up to 20 MeV, which is the upper limit of most cross sections available in evaluated nuclear data libraries. The current version 6 re-merged the X-branch of version 5 into the main development branch. As it also provides an optional cosmic-ray source, it has received considerable attention for calculations of the cosmic neutron spectrum.

GEANT4 (GEometry ANd Tracking) [Agostinelli et al. (2003)] can be regarded as a general-purpose, object-oriented successor to earlier high-energy transport codes, based on multithreaded C++ and OpenGL visualisation. It is designed specifically for the needs of high-energy and accelerator physics and excels at describing complex geometries. Because its interface requires programming skills, several wrappers such as TOPAS and GATE have been developed, particularly for clinical applications such as proton therapy. Since 2011, driven in part by the requirements of the European Spallation Source, an increasing number of low-energy neutron calculation capabilities have been introduced. There is now good agreement with other codes such as MCNP at low energies. However, although GEANT4 uses similar implementations for high-energy neutron transport, simulations of atmospheric propagation tend to predict systematically lower neutron fluxes at ground level.

At the Physikalisches Institut of Heidelberg University, the Monte Carlo code URANOS [Köhli et al. (2023), Köhli et al. (2025)] has been developed to address the specific needs of environmental physics and the CRNS method. This computationally efficient code simulates the relevant neutron interactions and uses a validated neutron source spectrum near the surface to minimise typical uncertainties associated with atmospheric propagation. A unique feature is its voxel engine, a geometry description based on three-dimensional pixels, which allows complex terrain to be modelled with a comparatively simple graphical data interface. In 2015, the understanding of cosmic-ray neutron transport at the soil–atmosphere interface was revised based on URANOS calculations, leading to a more precise effective model for the CRNS footprint as a function of environmental conditions related to various hydrogen pools.

Neutron simulation toolkits generally provide very similar results for the well-understood physics below 20 MeV, although there are differences in the underlying cross-section databases and high-energy transport models. Most codes agree within a few per cent at low energies. In our studies, we compared URANOS with the latest version (6.2) of MCNP and, in part, with GEANT4. In most scenarios they produced comparable results, with deviations of up to approximately 2 %, which can correspond to relative differences of around 10 % in derived quantities. There is a clear difference between the toolkits in the predicted flux changes for air humidity and soil moisture variations. URANOS yields an attenuation length in air similar to MCNP6, whereas the attenuation length in water in MCNP is slightly lower than in URANOS or than values suggested by cosmogenic nuclide studies (Nesterenok et al., 2012). As a result, high-energy neutrons are attenuated more rapidly in MCNP6, and the relative production of evaporation neutrons in the topsoil layers is higher. This could explain the identified differences in neutron flux between dry and moist conditions.

6.2 Modelling of SoMMet sites with the URANOS simulation code

All three high-level field sites are used in an agricultural context but differ greatly in soil and vegetation complexity. Furthermore, the measurement data available for comparison with simulation results varies significantly between the sites (see description above). On this basis, different goals were defined for the URANOS simulation campaigns at the three sites:

- **Bondeno:** Very generic agricultural setup with repetitive vegetation structures but heterogeneous soil density and moisture distribution; one long timeseries from a CRNS and a short time series using the ERBSS instrument of ASNR and W-PIE instrument of PoliMi.
  Goal of the study: Simulate the influence of soil density and, in particular, vegetation distribution on the epithermal neutron intensity and footprint dynamics and infer generic findings for similar sites.

- **Foggia:** Instrumentation similar to the Bondeno site. Limited land-use changes during the installation period, except for ploughing. The commercial CRNS device showed periods of malfunction and outage. Numerous sampling campaigns provide detailed input data for URANOS.
  Goal of the study: Reproduce the CRNS observations using data from these sampling campaigns.

- **Marquardt:** Highly instrumented field site with in-situ soil moisture data that provides comprehensive input for the simulation setup, and the longest BSS dataset of all three sites.
  Goal of the study: Compare simulated and measured neutron spectra for the full BSS time series.

Each virtual reconstruction of a site covered an area of 1 km^2 to avoid boundary effects. The total number of simulated neutrons was set to 100 million, which yielded between 10,000 and 50,000 detected neutrons for most setups and thus a relative statistical error of less than 1 %.

6.2.1 Bondeno site

<u>**Setup of the simulation domain**</u>

The simulation domain for the Bondeno high-level site in the URANOS code was built based on the following input data:

1. In situ soil sampling data from 72 sampling points arranged in three rings located at 3, 35 and 120 m distance from the sensor. Each ring includes six equidistant sampling locations, and at each location four samples were taken at depths of 2.5, 12.5, 22.5 and 32.5 cm.

2. Mean air temperature, humidity and pressure data from the cosmic-ray neutron detection system.

3. Biomass estimates derived from photographs and GIS (Geographic Information System) data.

A detailed soil bulk density map was inferred via linear interpolation of the sampling data within the horizontal and vertical sampling range, while the bulk density beyond 120 m distance was set to the sampling mean and, below 32.5 cm depth, to the in situ value at 32.5 cm. Figure 21 depicts the part of the test site (blue square) that was reconstructed in the URANOS' voxel engine. The model, visualised in Figure 22, includes a simplified representation of the structures within the simulation domain, including streets, ponds, buildings, grass, walnut tree trunks and canopy (see examples of layers in Appendix, Figure A 1).

A virtual detector is placed at the centre of the domain with a radius of 9 m and a height of 2.5 m to achieve a relative statistical error smaller than 1 % for each simulation setup. Trees are removed from the detector volume and its immediate vicinity (closer than 5 m) so as not to artificially increase the neutron track length in the detection region.

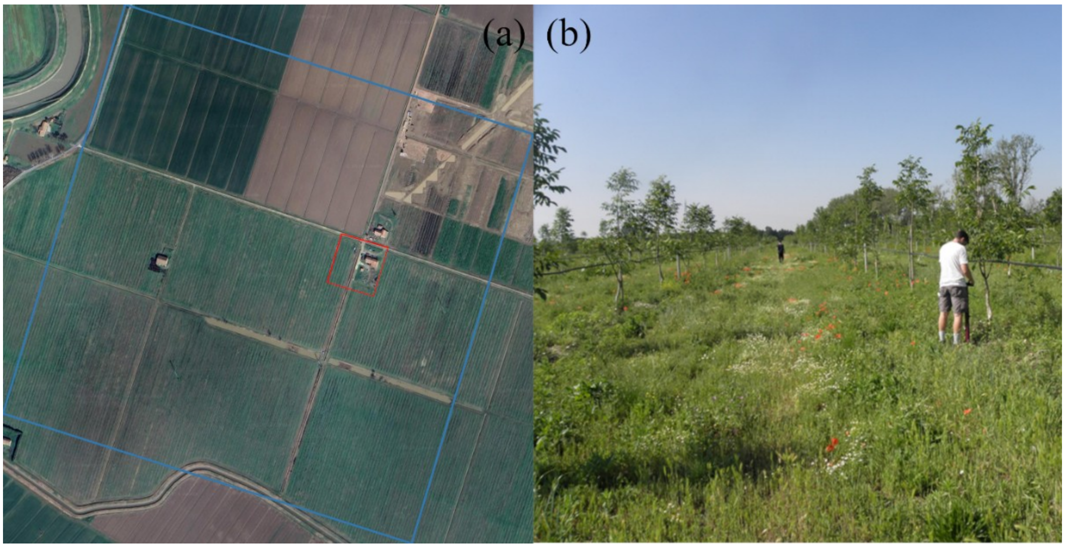

Figure 21. Bondeno site: (a) Birds-eye view of the site. The blue square marks the simulation domain of 1 km² while the red square designates the area for which the URANOS Input is exemplarily depicted in the figure below. The cosmic-ray neutron detector is situated in the center of the blue square. (b) Picture of the young walnut orchard at Bondeno.

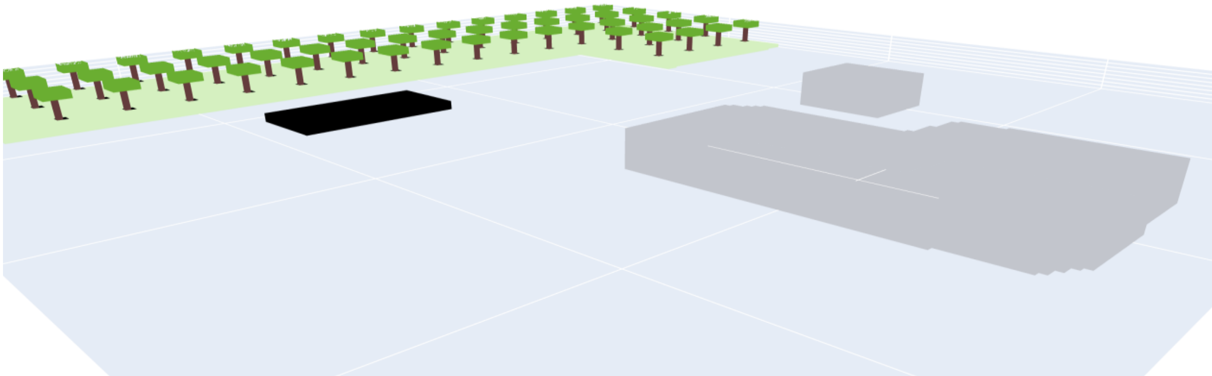

Figure 22. Bondeno site: Visualization of the URANOS input. The picture shows the 100x100 m selection marked in the subfigure (a) above. This cutout depicts trees and grass as well as two buildings in grey and a water pond in black.

Impact of vegetation and its spatial distribution on CRNS footprint characteristics

A range of different simulation setups was carried out to quantify the influence of specific substructures of the simulation domain on neutron transport, including:

1. Bare soil with a complex bulk-density pattern
2. Human-made structures: streets, buildings, ponds
3. Grass
4. Tree trunks
5. Tree canopy

Each simulation setup builds on the previous one, i.e. includes all virtual structures of the preceding setup and adds one additional structure type. All setups were run for ten soil moisture configurations: 1, 2, 3, 4, 5, 10, 20, 30, 40 and 50 vol. %. The R_{86}/R_{50} footprint radii range from 220/61 m for bare soil and a volumetric soil moisture of 1 % to 166/29 m for scenarios 5 and 50 vol. %. Streets, buildings and even ponds have a negligible effect on the CRNS footprint at the Bondeno site, as they are located relatively far from the sensor (ponds > 170 m, street > 140 m, buildings > 200 m). By contrast, grass and walnut trees change the footprint significantly, as they surround the neutron sensor, as shown in Figure 23. A reduction in footprint size with increasing biomass water equivalent (BWE) can be observed, similar to the effect of air humidity (Köhli et al., 2015). Furthermore, within the range investigated in this study, soil moisture changes have a much stronger impact on the overall footprint size than BWE.

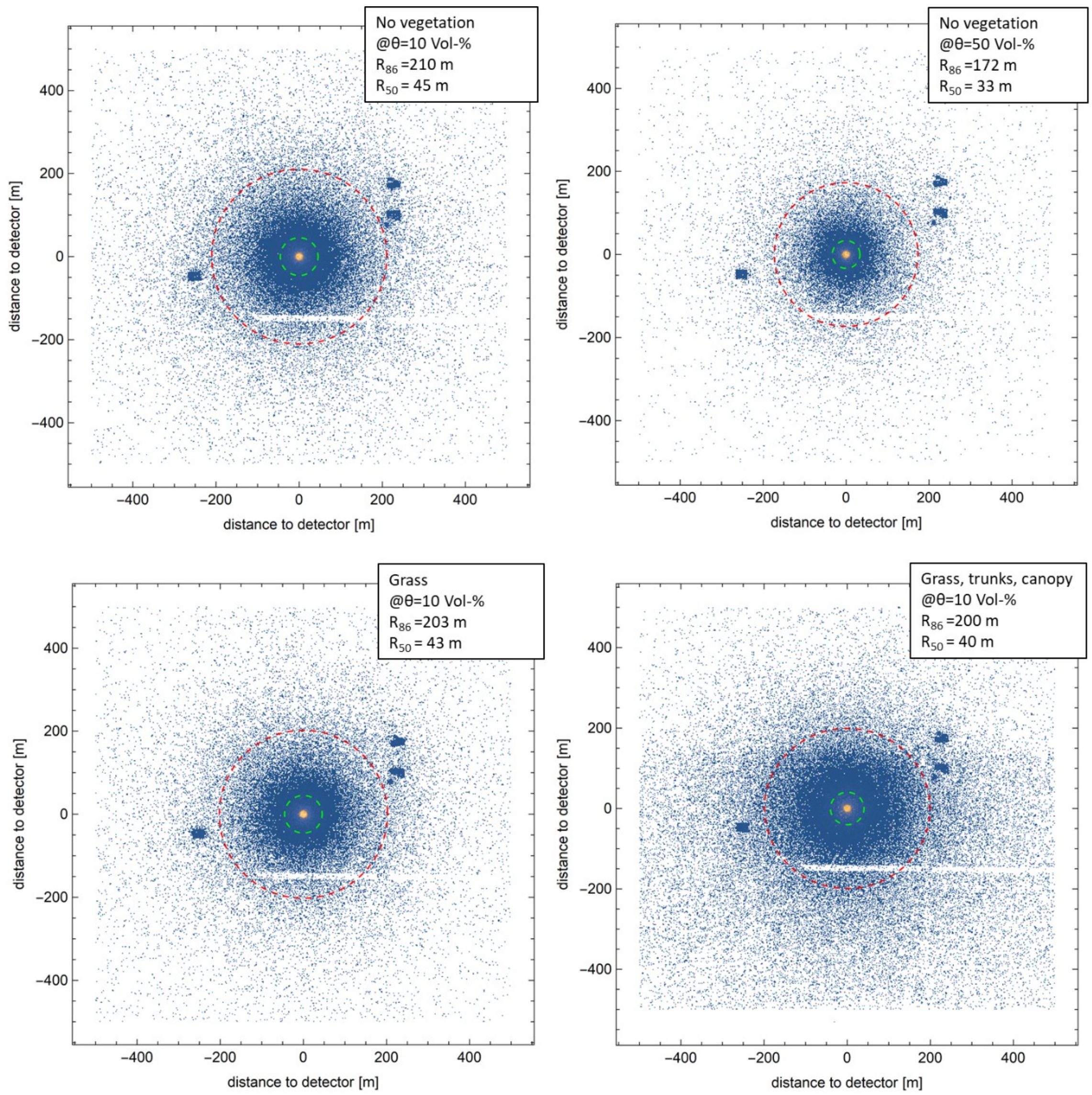

Figure 23. Four examples of neutron-soil interaction heat maps (blue indicates single while yellow indicates higher density of interactions). The R_{50} and R_{86} footprint radii are indicated with a green and red dotted dashed circle, respectively.

Table 2 reveals more detailed aspects of how the spatial distribution of BWE influences the footprint size. First, it should be noted that homogeneously distributed biomass, such as grass, leads to a stronger footprint reduction per kg m^{-2} than sparsely distributed tree trunks. The spatial homogeneity of a medium is directly linked to the penetration and thus the interaction probability of neutrons within it, which explains this unequal influence of different biomass types.

Moreover, grass and tree trunks decrease the R_{50} footprint size because the local neutron transport is predominantly geometric, i.e. neutrons travel directly from the soil to the detector. Any material located in the line of sight between soil and detector, and having a higher macroscopic scattering cross section than air, will reduce the probability of this direct transport. By contrast, the tree canopy is located above the sensor and therefore does not significantly affect this direct geometric transport. As a result, the tree canopy has little influence on local footprint dynamics, but it does affect long-range neutron transport, which is characterised by multiple scattering and extends vertically beyond the sensor height.

Table 2. Changes in footprint size for three different vegetation scenarios of the Bondeno site (see text). Second column shows the decrease in R50 and R86 footprint size as compared to the bare soil scenario at a soil moisture content of 10 Vol-%. Columns three and four indicate the total BWE (biomass water equivalent) amount and change to the previous scenario and the area coverage of the added vegetation compartment (area coverage of grass and trunks only show that of the tree trunks). Finally, the relative change in R_{50} / R_{86} with respect to the added BWE is shown in the last column.

Vegetation scenario @θ=10 Vol-%	**R_{50}/R_{86} decrease [%]**	**BWE total/increase [kg/m²]**	**Area coverage [%]**	**R_{50}/R_{86} change per BWE [%/(kg/m²)]**
grass	4/2.5	0.2/0.2	100	20/12.5
grass & trunks	15/5	1.8/1.6	0.6	7/1.5
grass, trunks & canopy	15/5.5	2/0.2	15	<0.1/2.5

Impact of vegetation on the epithermal intensity

The epithermal neutron intensity at a virtual detector placed at the centre of the simulation domain was calculated for all simulated setups (see list above), using the validated detector response function of the CRNS probe Finapp 3 (see Deliverable D2). A decrease in intensity with increasing biomass water equivalent (BWE) can be observed for dry to moderately wet soils (see Figure 24). However, this effect diminishes and can even invert for wet soils, as the soil becomes similarly rich in hydrogen as the overlying biomass and the additional impact of biomass on top of a wet soil becomes negligible.

In the URANOS model, the virtual biomass is represented by cellulose ($C_6H_{10}O_5$) and air. Within the range investigated here, the effect of BWE on the CRNS signal is significant but almost one order of magnitude smaller than that of soil moisture. Overall, its influence is similar to that of air humidity, with two important differences: the water density in biomass can greatly exceed that in air, and biomass can exhibit a much more heterogeneous spatial distribution. Consequently, an adaptation of the universal transport function (UTS; Köhli et al., 2021), analogous to the air-humidity terms, is introduced to obtain an analytical description of the intensity:

$$e^{(-p_3\theta)}p_4 + (p_1 + p_2x)/(p_1 + x) \ ,$$

with the parameter set given in Table 3.

Table 3. Parameter sets used to adapt the Universal Transport Solution (UTS) for different vegetation scenarios.

Vegetation scenario	p1	p2	p3	p4
No vegetation	5.97	0.17	0.84	0.28
grass	6.20	0.18	0.86	0.27
Grass & trunks	6.59	0.19	0.78	0.23
Grass, trunks & canopy	6.41	0.20	0.77	0.22

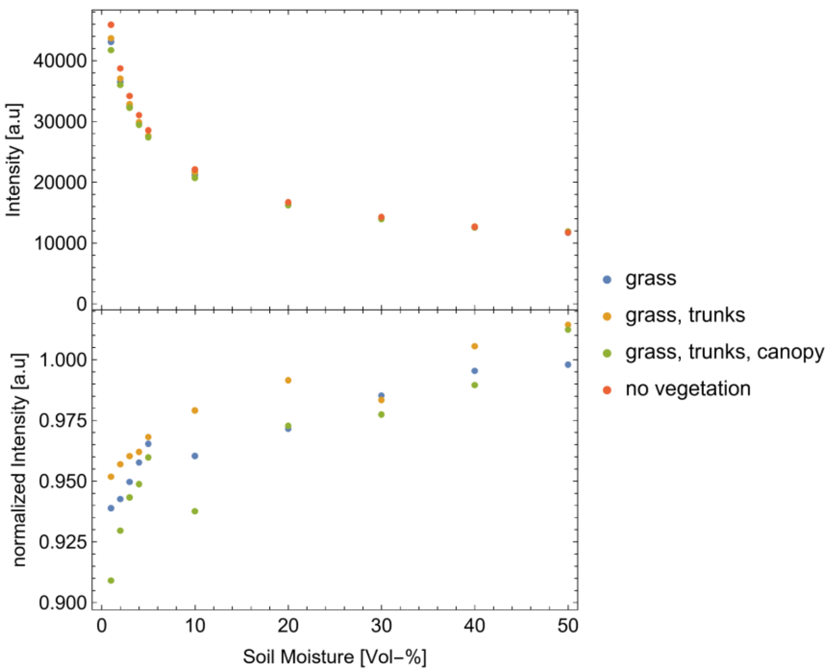

Figure 24. Simulated intensities of a virtual detector for different vegetation scenarios as a function of soil moisture. Top panel: Absolute intensities. Bottom panel: Intensities normalized to the simulation scenario without any vegetation.

6.2.2 Foggia site

Setup of the simulation domain

The geometric setup of the Foggia high-level site has remained relatively constant throughout the period of CRNS data acquisition. Therefore, a single structural model was constructed from satellite imagery and GIS data and used for all simulations. This model consists mainly of a thin grass layer, streets, several buildings and trees (see Figure 25). In contrast to the Bondeno site, Foggia does not feature large BWE pools in the immediate vicinity of the sensor. Hence, the dominant driver for changes in the measured epithermal neutron intensities is the ratio between water and dry matter in the soil, which is controlled by both changes in volumetric soil moisture and changes in bulk density due to ploughing.

The simulation domain for the Foggia site is visualised in Figure 26 (examples of the layers can be found in Appendix, Figure A 2). The simulation setups were based on eleven sampling campaigns with multiple bulk density and volumetric soil moisture samples at twelve different locations. Both bulk density and volumetric moisture content were interpolated and extrapolated within the bounds of the field indicated by the pink polygon shown in Figure 25. Beyond this area, constant values representing the respective averages were assumed for both quantities.

Comparison of simulation results and measured data

Similarly to the Bondeno case, the URANOS output spectra were weighted with the corresponding detector response function to obtain a realistic representation of the actual detector neutron count rate. The CRNS time series contain data gaps as well as noisy intervals, but the moistening of the soil during late summer and autumn can clearly be observed both in the simulation results and in the CRNS epithermal channel (Figure 27, panel (a)). The R_{86}/ R_{50} footprint radii reach their maximum in late August, with values of 198 m and 44 m, respectively, and decrease to 167 m and 33 m by the end of October. The corresponding penetration depths D_{86} lie between 20 and 35 cm.

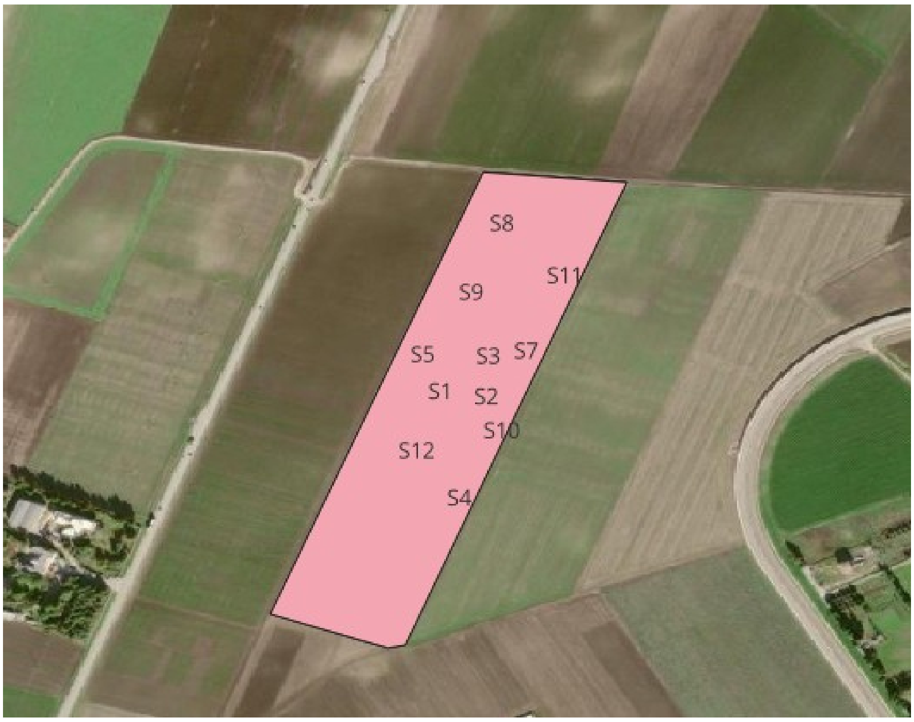

Figure 25. Satellite image exported from QGIS of the 1 km² simulation domain for the Foggia high-level site. The CRNS probe is located in the centre of the figure between S1 and S2. S1-S12 denote the sampling locations.

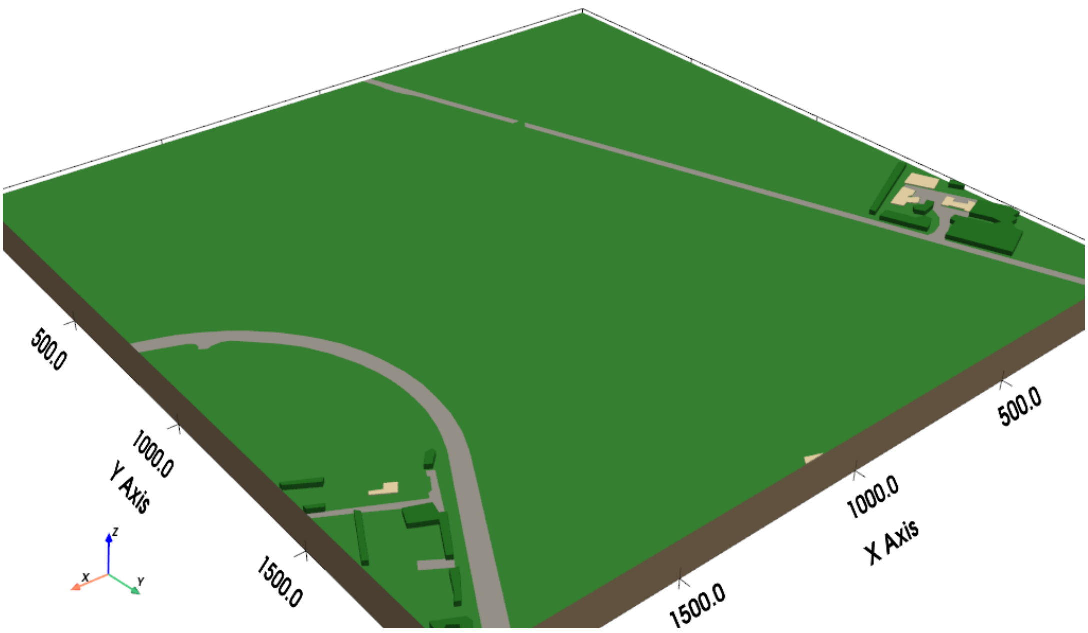

Figure 26. Setup of the 1 km² Foggia simulation domain as URANOS input extracted from the GIS data in Figure 25.

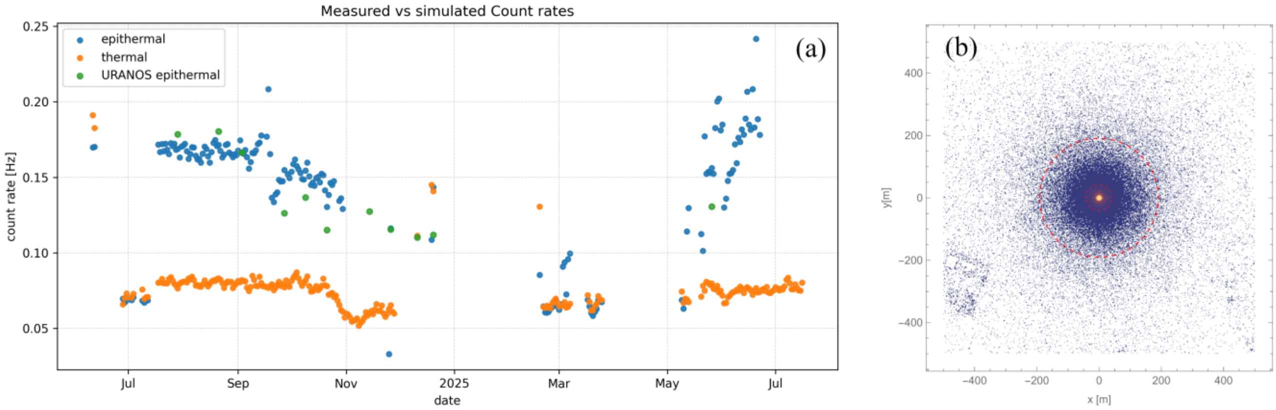

Figure 27. (a) Measured epithermal and thermal count rates vs simulated epithermal count rates (weighted with a detector response function). The data from eleven intensive soil sampling campaigns served as the basis for the highly resolved input matrices for the URANOS simulation setups. The CRNS device shows malfunction and failure for large parts of the time series. (b) Exemplary plot of simulated neutron soil interaction prior to the neutron's detection shows the footprint dynamics during the sampling campaign of the 29th of Sep 2024.

6.2.3 Marquardt site

Setup of the simulation domain

Over a period of six years, more than 147 soil samples (0–35 cm depth, in 5 cm increments) were collected, including measurements of bulk density. These data were used to create an interpolated bulk density map using inverse distance weighting (IDW).

At CRNS station #31 (StyX Neutronica), a spatial soil moisture survey was carried out using FDR sensors (0–35 cm, 5 cm increments) across 20 profiles. The resulting soil moisture distributions were compared with continuous profile sensor data at the same location, yielding 121 time-steps (12-hour intervals, 1 June–31 July 2025) of spatial soil moisture maps. In addition, 26 soil samples from across the site were analysed for lattice water and organic matter content. These parameters were assumed to be spatially static, and their mean values were applied across the entire study area.

For aboveground structures (such as trees and buildings), a normalised Digital Surface Model (nDSM) was created and classified using custom polygons. The structures were modelled in vertical increments up to 30 m to capture canopy and building variability in detail. Subsurface layers were represented in 1 cm steps down to 14 cm, with additional layers at 50 and 150 cm depth, allowing high-resolution integration of soil and vegetation structure information. All generated maps have a spatial resolution of 1 m and an extent of 1 km^2, with CRNS sensor #31 located at their centre (see Figure 28). Two example matrices are shown in Appendix, Figure A 3.

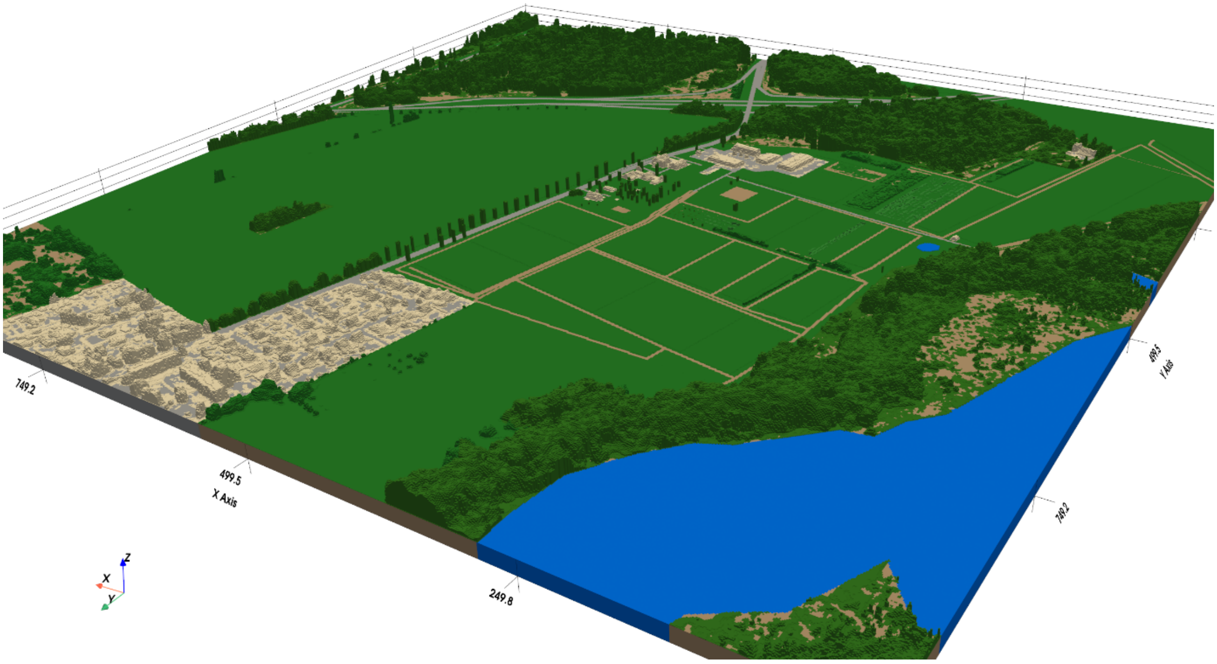

Figure 28. Representation of the simulated geometry in URANOS. Each vertical grid layer is provided as input, and the neutron detector is modelled at the centre of the domain.

Comparison of time series: simulated and measured neutron spectra

The time series of neutron count rates recorded by the individual Bonner spheres of the NEMUS-UMW set were analysed and corrected for variations in air pressure and incoming radiation, using data from the neutron monitor in Kiel, chosen due to its proximity and sea-level altitude. Figure 29 shows the corrected and filtered neutron count rate time series for each sphere. Based on the recorded count rates, the neutron spectra were derived using unfolding procedures and compared with the simulated spectra (see Figure 30). To enable this comparison, the simulation was normalised to the evaporation neutron peak of the unfolded BSS measurement. Figure 30 also shows the comparison of neutron fluxes in the thermal, epithermal, fast and high-energy regions.

Monitoring and quantification of precipitation events at the Marquardt site, together with soil moisture datasets collected using commercial point-scale sensors, allow the changes in the individual Bonner spheres and the dynamics observed in the entire time series to be interpreted: The significant decrease in the epithermal and fast energy ranges on 12 July 2025, clearly visible in both Figure 29 and Figure 30, is attributed to the first heavy rainfall that occurred after the start of Bonner sphere data taking with the NEMUS-UMW system. The corresponding change in the neutron energy distribution before and after this precipitation event can be attributed to changes in soil moisture in the area. The increased moderation of neutrons is due to the higher abundance of water (and its hydrogen atoms) in the soil following precipitation, resulting in a shift of neutron fluence from epithermal to thermal neutrons, while the high-energy part of the neutron distribution remains unchanged. This illustrates the mechanism underlying CRNS observations of water content via the detection of epithermal neutron fluence rates.

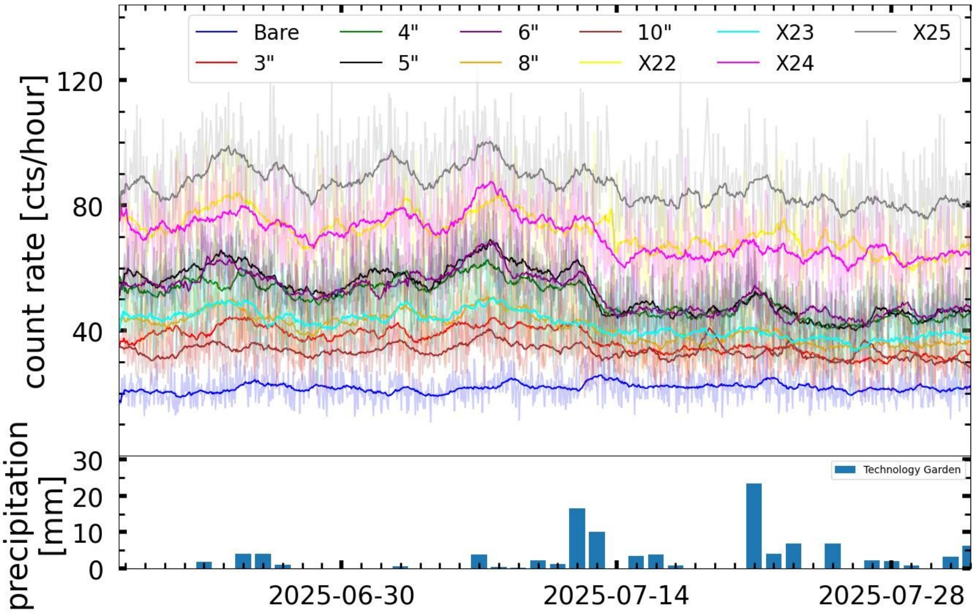

Figure 29. Neutron count rates measured with the individual Bonner spheres of PTB's NEMUS-UMW system at the Marquardt site. Upper panel: time series of count rates, already corrected for fluctuations in incoming cosmic radiation and atmospheric pressure. Solid lines denote the 24-hour rolling average. The spheres designated "X" are modified with additional lead or copper shells to detect high-energy neutrons. Lower panel: locally measured precipitation.

The simulated neutron spectra, derived with the URANOS code based on the simulation domain and the point-scale soil moisture datasets, also predict this decrease in epithermal and fast neutron count rates. In addition, a significant but relatively small drop in intensity is visible in the simulated thermal neutron energy region. However, it should be noted that the simulation-based results exhibit large uncertainties, because small abundances of strong neutron absorbers in soil such as boron or gadolinium can, in principle, substantially reduce the thermal neutron flux. In fact, the simulated thermal neutron intensities were artificially reduced to 80 % of their original value to account for this effect. The second precipitation event on 21 July 2025 leads to a much less pronounced effect in the epithermal and fast energy ranges, because the soil was already moist, but the impact is still observable in both the simulated and unfolded datasets.

The time series of the individual Bonner spheres with diameters of 3, 4 and 5 inches were also directly compared (without unfolding the full neutron energy spectrum) with the neutron count rate measured by stationary CRNS system #31, which is part of the CRNS cluster at the Marquardt site. Such a comparison is feasible because the neutron response functions of the smaller-diameter Bonner spheres are very similar to the characteristic response of commercial CRNS systems. This comparison, shown in Figure 31, reveals a pattern consistent with the measured–simulated comparison described above: a marked decrease in neutron count rate following the first heavy precipitation event, and a smaller decline after the second event.

Overall, it has been demonstrated that a well-controlled and well-characterised ERBSS system such as PTB's NEMUS-UMW has the potential to validate neutron time series measured with neighbouring CRNS detectors and to collect datasets that are suitable for systematic benchmarking of the URANOS simulation code.

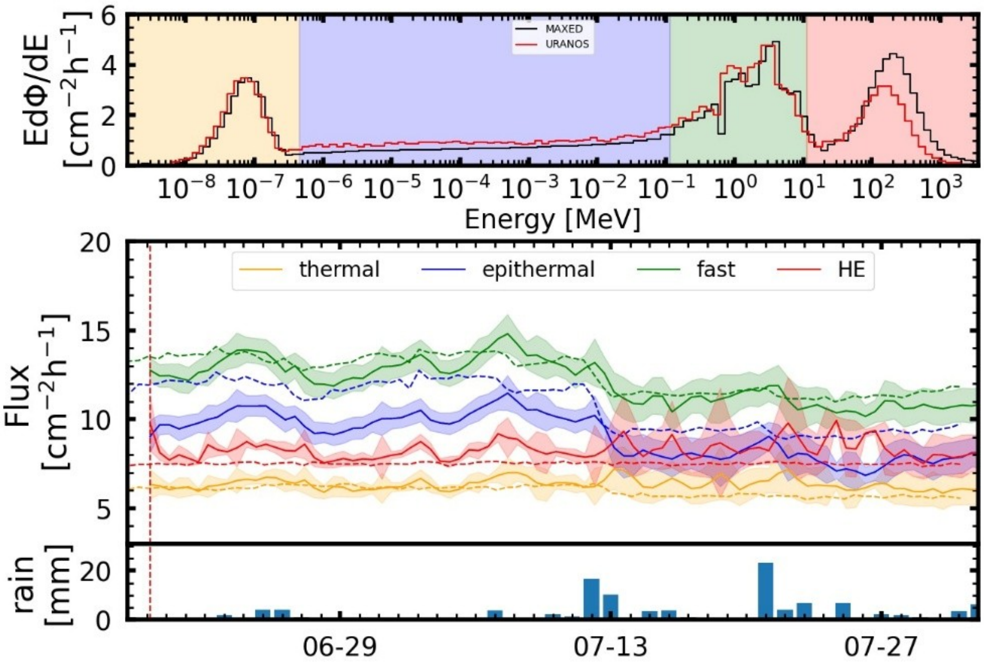

Figure 30. Time series of the neutron fluence rate in absolute units (n cm^{-2} s^{-1}) in four neutron energy regions: thermal, epithermal, fast and high-energy neutrons. Top panel: simulated neutron spectrum from URANOS (red) and unfolded spectrum derived from NEMUS-UMW Bonner sphere data using the MAXED unfolding algorithm at the beginning of the time series. Bottom panel: time series of simulated (dashed lines) and measured/unfolded (solid lines) neutron fluence rates in the individual neutron energy ranges, accompanied by the precipitation time series shown at the bottom.

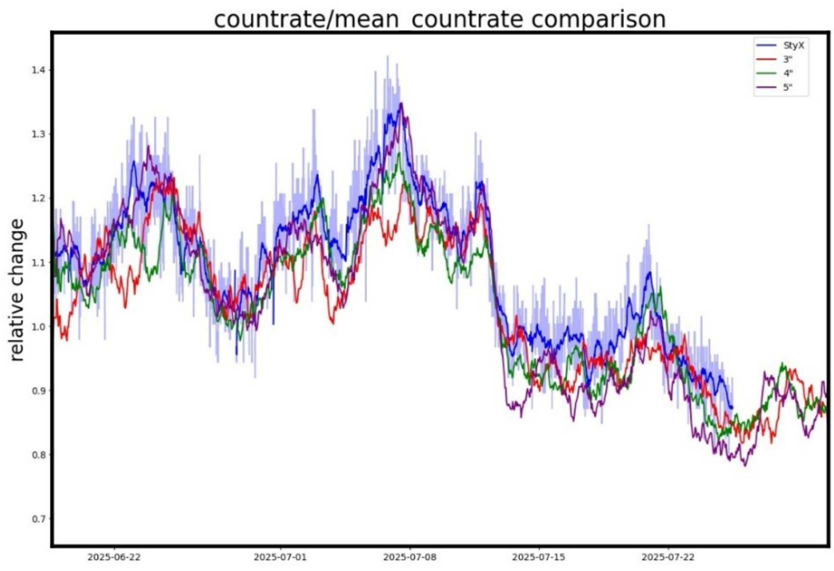

Figure 31. Count rate comparisons between a stationary CRNS probe and the 3-, 4- and 5-inch Bonner spheres of the NEMUS-UMW system. The absolute values differ greatly between the large CRNS device and the smaller Bonner spheres and have been normalised for better visualisation.

6.3 Benchmarking of URANOS digital twin models with ERBSS datasets

A time series comparison between the URANOS model and the ERBSS data for the Marquardt site was presented in the previous section. Here, the focus is on systematic differences, the uncertainties of both the simulations and the ERBSS measurements, and on how a simulation benchmark can be derived from the experimental data.

Before a dedicated comparison between measured and simulated results can be carried out, the major sources of uncertainty for both need to be understood. In the case of URANOS as a Monte Carlo code, these include:

- **Neutron input spectrum:** URANOS starts casting particles from an energy and angular spectrum taken from Sato (2016). Any uncertainty in this spectrum is directly propagated into the simulation results.
- **Absolute vs. relative flux:** URANOS does not natively compute absolute fluxes but is primarily used as a toolset to analyse relative changes in neutron intensity due to varying environmental conditions.
- **Nuclear data:** Neutron cross sections are fairly well known in the evaporation and epithermal energy regime and, although more angularly complex, also in the thermal energy regime. At higher energies, both cross sections and effective evaporation and spallation models exhibit significantly larger uncertainties.
- **Effective production models:** Beyond the input spectrum mentioned above, URANOS generates neutrons via effective models that represent neutron production by evaporation and spallation of high-energy cosmic rays.
- **Domain setup:** Uncertainties in the domain setup induce errors in the neutron flux. This includes limited geometric detail in the representation of the environment as well as uncertainties in the chemical composition of the materials used. The latter can have a major impact on absorption characteristics and, to a lesser extent, on neutron evaporation properties.

On the other hand, the ERBSS measurement data and its translation into neutron spectra inherit the following uncertainties:

- **Counting statistics:** The Bonner sphere detectors have relatively low counting statistics, with count numbers typically in the range of 20 to 100 neutron counts per hour.
- **Unfolding procedure:** The unfolding process introduces an additional uncertainty budget that mainly originates from the low statistics and the dependence on the assumed initial (prior) spectrum.
- **Sensitivity to other particles:** Bonner spheres with a neutron producer are inherently sensitive to other hadrons and, to a lesser extent, muons via neutron production in the converter material.

Putting the above lists into perspective, one can already conclude that ERBSS data can be used as a benchmark for URANOS in at least two ways:

- To link relative changes in neutron flux from URANOS simulations to absolute values.
- To constrain and understand the thermal neutron intensity relative to the remaining spectrum.

While epithermal neutrons are the main tool to monitor environmental hydrogen pools, thermal neutrons have been used in numerous studies to detect biomass water content. However, the thermal energy regime is strongly affected by both scattering and absorption processes. Strong absorbers such as boron and gadolinium can significantly reduce the thermal neutron intensity and its dynamics, even when present only at concentrations of a few ppm. Typically, the concentration of these absorbers remains relatively constant if they are not applied as fertilisers (which can be the case for boron). Thus, a single ERBSS measurement can help to identify the total neutron absorption potential of the soil and thereby improve CRNS-based biomass retrieval.

Two spectra, both simulated and unfolded, are shown in Figure 32, representing dry and wet conditions before and after the heavy precipitation event on 12 July 2025 at the Marquardt site (see also the previous section). The simulated spectra were scaled to the absolute values of the ERBSS spectra using the integral over the fast energy regime. The simulated thermal neutron peak was reduced to 80 % of its original intensity in order to account for unknown, and therefore not explicitly modelled, absorbers in the soil. Measured and simulated data agree well, except for the high-energy range (energies higher than 20 MeV). The higher values in the unfolded spectra are expected to originate mainly from contributions of other particle species to neutron production in the spheres' converters, whereas the simulated spectra represent only the neutron component of the cosmic-ray flux. Uncertainties in the input spectrum and in high-energy cross sections may further contribute to these differences.

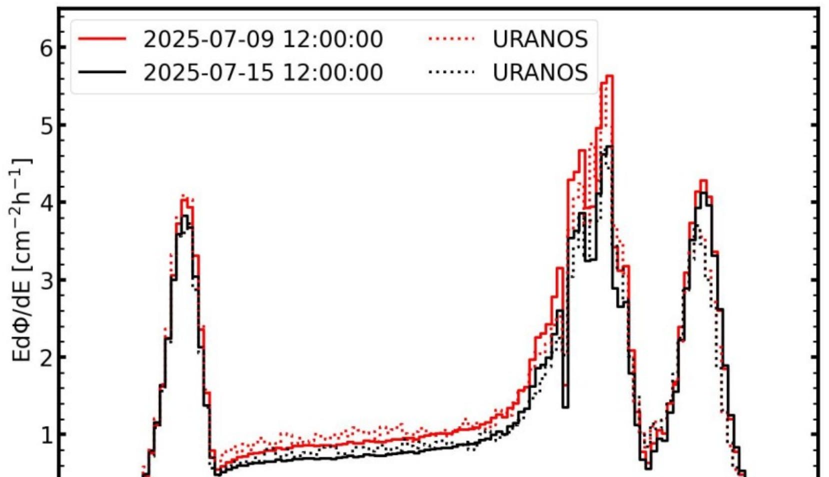

Figure 32. Comparison of URANOS-simulated (dashed line) and unfolded (solid line) neutron spectra before (2025-07-09) and after (2025-07-15) the first heavy precipitation event observed during the measurement campaign in Marquardt. The unfolded spectra result from the analysis of datasets recorded with the NEMUS-UMW Bonner sphere system.

7 Concept of a virtual reference CRNS neutron field: coupling URANOS site models with device-specific CRNS digital twins

In deliverable D2, the selected CRNS probes were modelled using the MCNP Monte Carlo transport code, and these models were successfully validated under laboratory conditions in well-characterised neutron reference fields. However, the actual operating conditions in the field differ in both the energy and angular distributions of the neutrons: outdoor operation exposes a CRNS system to a much more complex irradiation environment than that encountered in the laboratory.

Therefore, to meaningfully intercompare the responses of different CRNS probes under outdoor conditions, it is necessary to do so under well-defined and harmonised conditions that realistically approximate their real operating environment. This intercomparison was carried out via a dedicated Monte Carlo-based simulation study, in which the laboratory-validated digital twin models of the CRNS systems were coupled with a URANOS-based simulated environment that mimics, as closely as possible, the conditions encountered outdoors. The novel underlying concept, developed by UHEI and CMI, is referred to as a “virtual reference CRNS neutron field”.

7.1 Definition of the virtual reference CRNS field

To assess the behaviour of the tested CRNS probes in the relevant operation conditions, the concept of a virtual reference CRNS field is introduced. This field was calculated using URANOS neutron transport code with following planar, horizontally homogeneous geometry:

Soil parameters:

- Depth: 1.7 m
- Soil composition (see also [Köhli et al. (2015)]:
  - The soil consists of 50 % vol. solids and a scalable amount of H_2O.
  - The solid phase is composed of 75 % vol. SiO_2 and 25 % vol. Al_2O_3 at a compound density of 2.86 g/cm^3.
  - The total bulk density depends on the volumetric water content, e.g. 1.43 g/cm^3 for 0 % volumetric water content and 1.93 g/cm^3 for 50 % volumetric water content.
  - A volumetric water content of 100 % represents a theoretical case without a solid phase, i.e. the entire “soil” volume is composed of water.

Atmosphere parameters:

- Thickness: 1600 m
- Air composition (see also [Köhli et al. (2015)]:
  - 78 % vol. nitrogen, 21 % vol. oxygen, and 1 % vol. argon at a pressure of 1020 mbar
  - Air humidity of 10 g/m^3

Neutron source parameters:

- Horizontal extent (domain diameter): 800 m
- Source height: 650 m
- Source neutron spectrum shown on Figure 33, see also [Köhli et al. (2015)]

- Source neutron directional distribution, see [Sato et al. (2006)]
- Cut-off rigidity: 5 GV

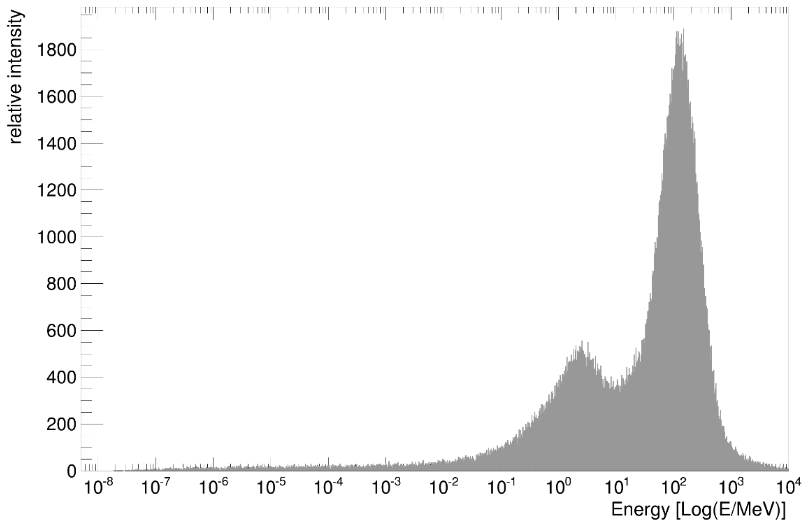

Figure 33. Primary neutron energy spectrum at 650 m above the ground used by URANOS calculation to calculate energy, position and angular distribution of the neutrons on the surface of the virtual sphere 2 m in diameter.

In the centre of the domain, a virtual sphere with a diameter of 2 m was placed, with its centre located 1 m above the soil surface (see Figure 34). This position corresponds to the centre of a CRNS probe installed at the recommended height, i.e. 1 m above ground level. Every simulated neutron crossing the surface of this sphere was recorded, thereby defining the so-called ***virtual reference CRNS neutron field***.

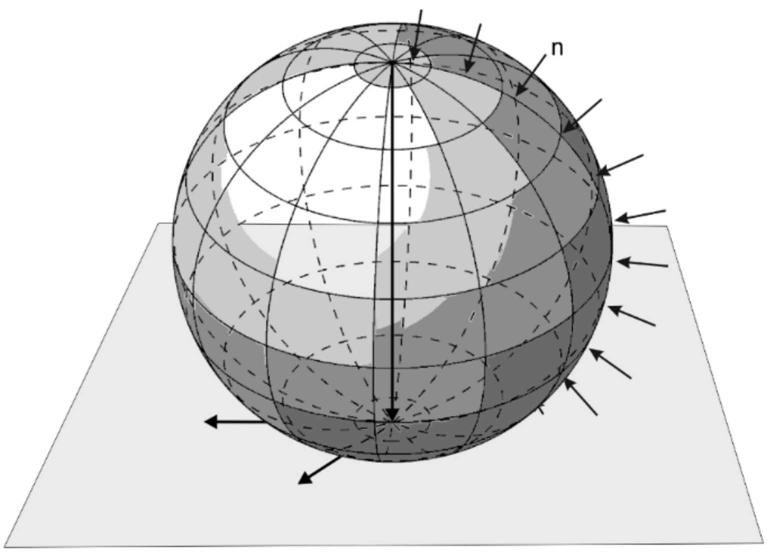

Figure 34. Virtual sphere 2 m in diameter used for the calculation of reference CRNS neutron field as well as a neutron source for the detailed MCNP calculation of CRNS probe responses.

The virtual fields generated exist in two different forms: one as a source definition for detailed MCNP calculations (a pseudo PTRAC file (Particle Track Output)), and one as the original URANOS output. In both cases, the neutron energy, the point of intersection of the neutron with the sphere, and the directional vector are recorded. In the URANOS output, the neutron's origin (used to calculate the CRNS footprint) and its last interaction point before entering the sphere are also stored.

The footprint radius and the support volume depth—that is, the region from which the CRNS probe effectively senses the signal—vary with soil moisture. Typical ranges are approximately (140–240) m for the radius and (15–75) cm for the depth.

In total, nine virtual reference CRNS neutron fields were prepared for nine different volumetric soil moisture values of 1 %, 3 %, 6 %, 10 %, 20 %, 30 %, 40 %, 50 % and 100 %, assuming a constant air humidity of 10 g/m^3. The last case, 100 % soil moisture, represents a theoretical limiting situation with no solid phase in the soil, i.e. the entire "soil" volume is composed of water.

7.2 Neutron distribution on the virtual sphere

In total, nine virtual reference CRNS neutron fields were prepared for nine different volumetric soil moisture values of 1 %, 3 %, 6 %, 10 %, 20 %, 30 %, 40 %, 50 % and 100 %, assuming a constant air humidity of 10 g/m^3. The main parameters of these neutron fields are summarised in the following plots: Figure 35 to Figure 43.

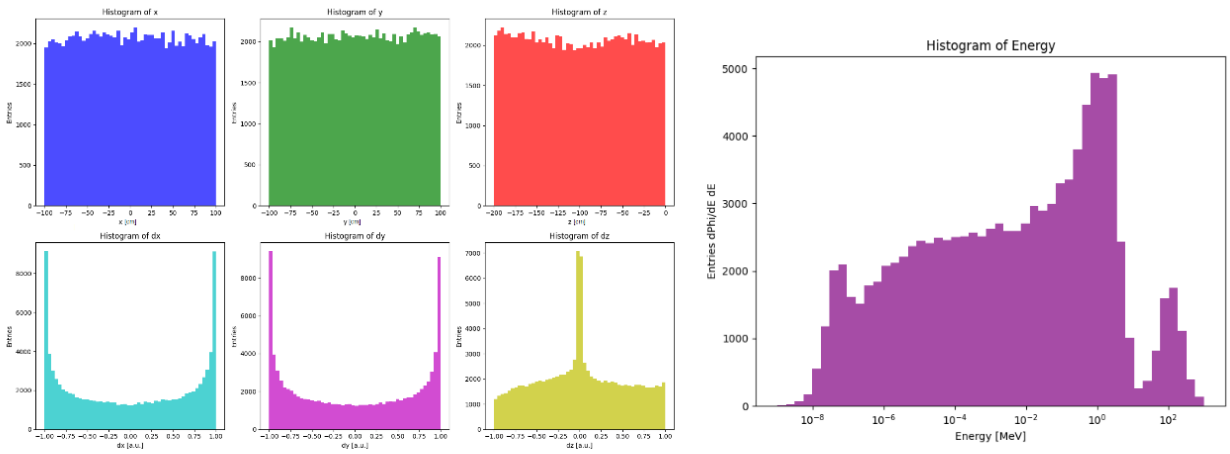

Figure 35. Relative volumetric soil moisture of **1 %**. Left: Histograms of simulated neutron entries along the *x*-, *y*- and *z*-axes, respectively. Right: Neutron energy spectrum. Simulation performed with a total of 3.1×10^9 initial neutrons.

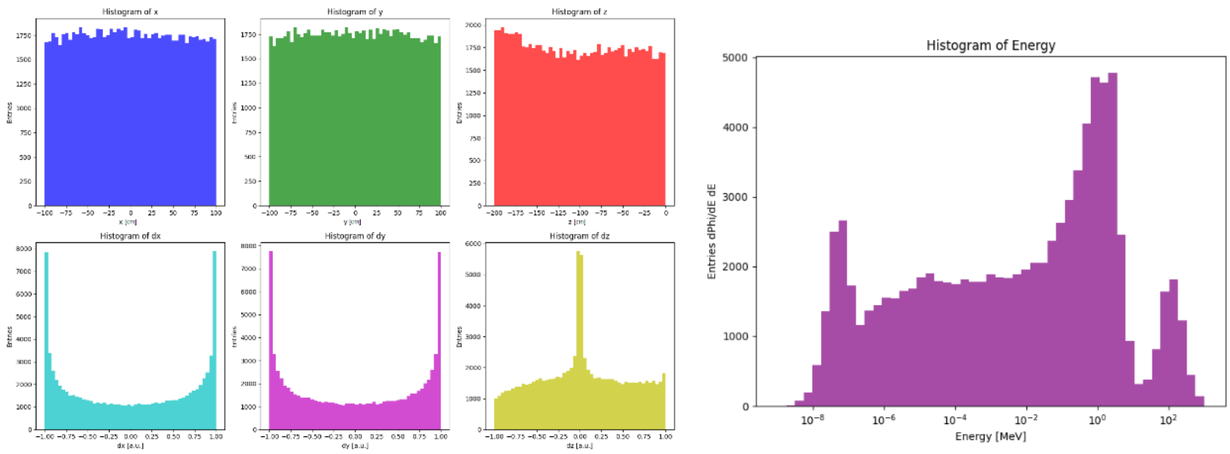

Figure 36. Relative volumetric soil moisture of **3 %**. Histograms of calculated neutron entries with respect to particular axis (left). Neutron energy spectrum (right). Simulation performed with a total of 3.2×10^9 initial neutrons.

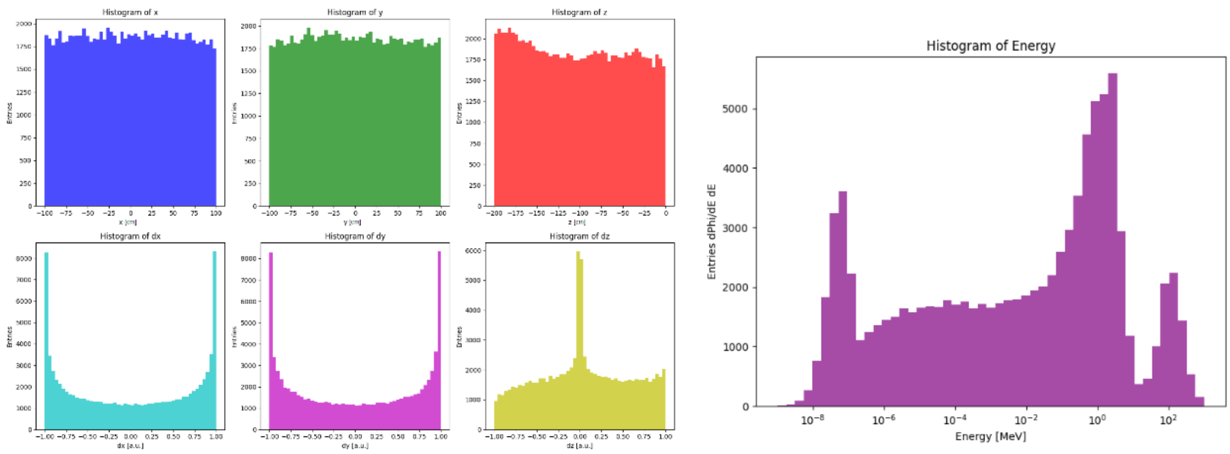

Figure 37. Relative volumetric soil moisture of **6 %**. Histograms of calculated neutron entries with respect to particular axis (left). Neutron energy spectrum (right). Simulation performed with a total of 4.0×10^9 initial neutrons.

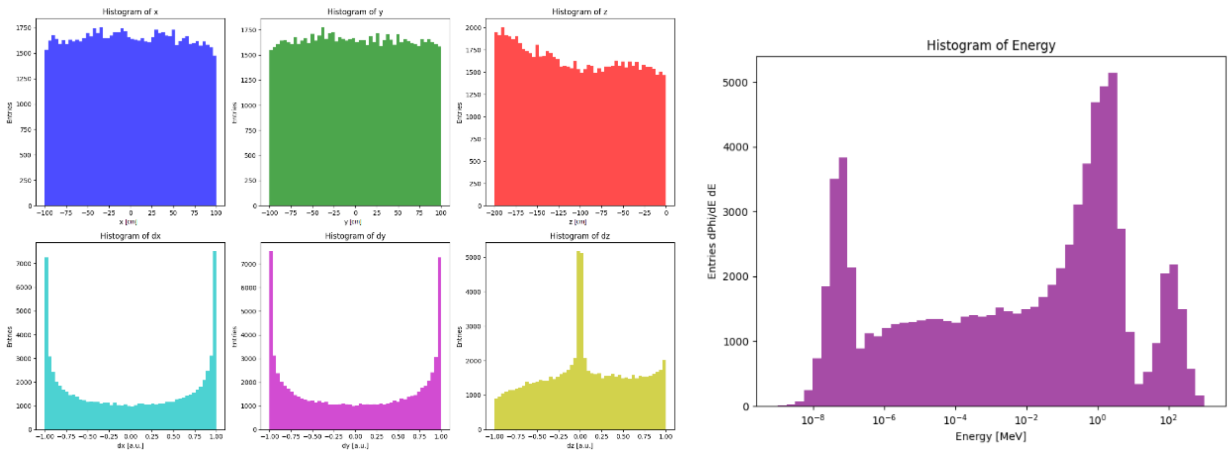

Figure 38. Relative volumetric soil moisture of **10 %**. Histograms of calculated neutron entries with respect to particular axis (left). Neutron energy spectrum (right). Simulation performed with a total of 4.0×10^{9} initial neutrons.

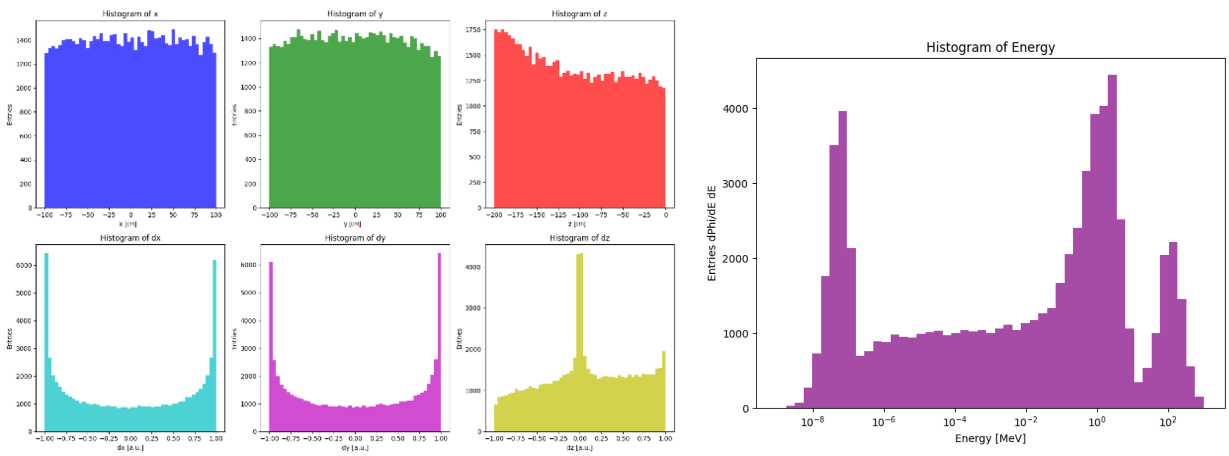

Figure 39. Relative volumetric soil moisture of **20 %**. Histograms of calculated neutron entries with respect to particular axis (left). Neutron energy spectrum (right). Simulation performed with a total of 4.0×10^{9} initial neutrons.

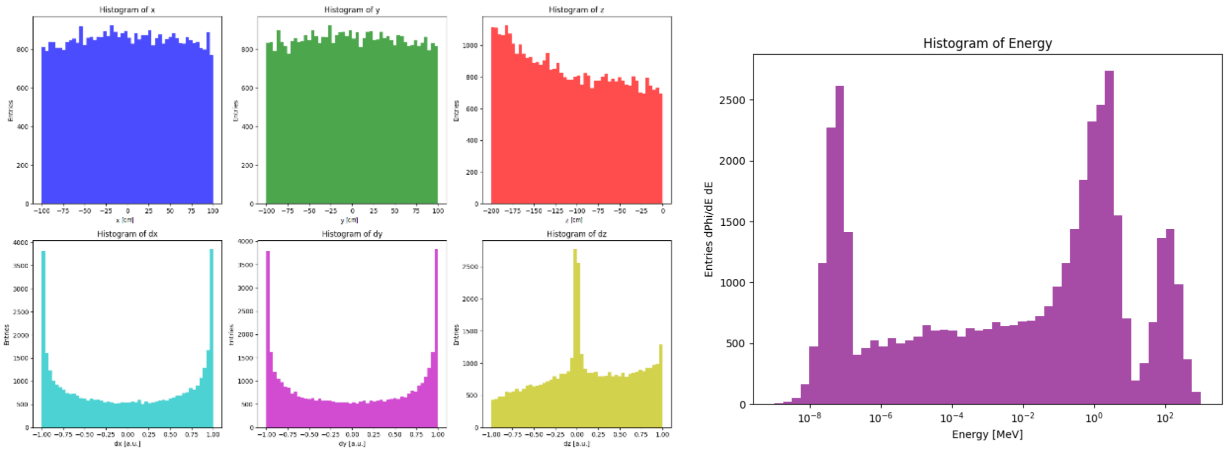

Figure 40. Relative volumetric soil moisture of **30 %**. Histograms of calculated neutron entries with respect to particular axis (left). Neutron energy spectrum (right). Simulation performed with a total of 2.7×10^{9} initial neutrons.

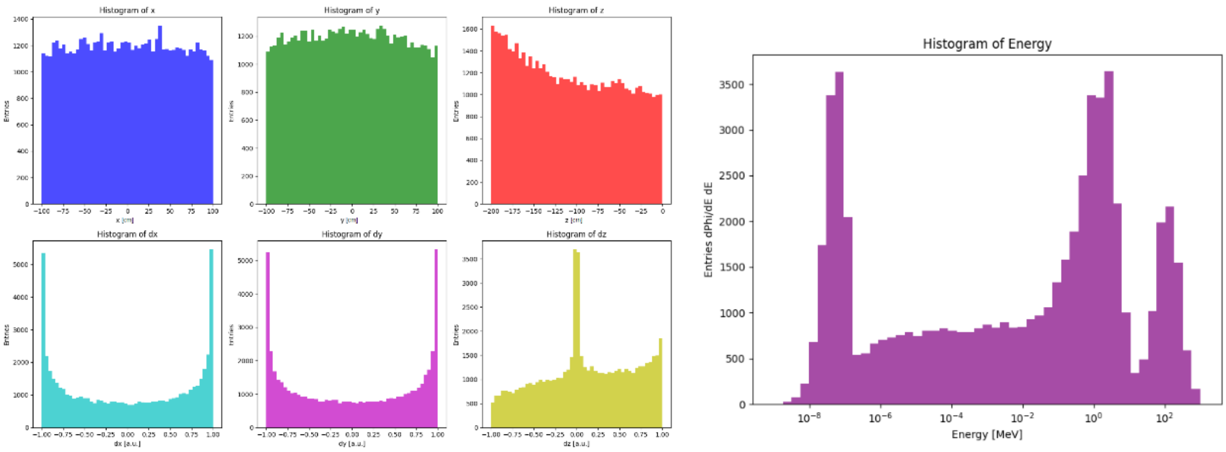

Figure 41. Relative volumetric soil moisture of **40 %**. Histograms of calculated neutron entries with respect to particular axis (left). Neutron energy spectrum (right). Simulation performed with a total of 4.0×10^{9} initial neutrons.

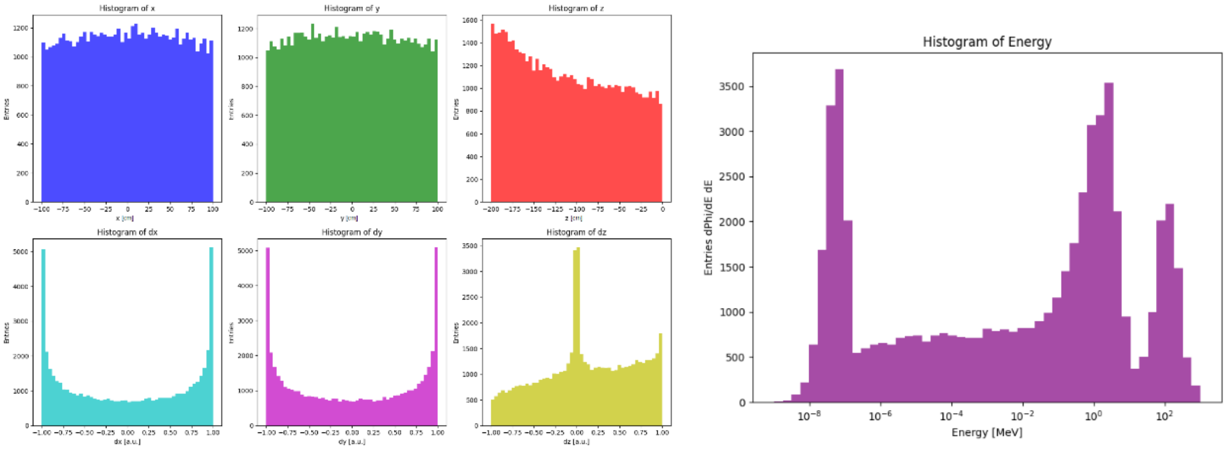

Figure 42. Relative volumetric soil moisture of **50 %**. Histograms of calculated neutron entries with respect to particular axis (left). Neutron energy spectrum (right). Simulation performed with a total of 4.0×10^9 initial neutrons.

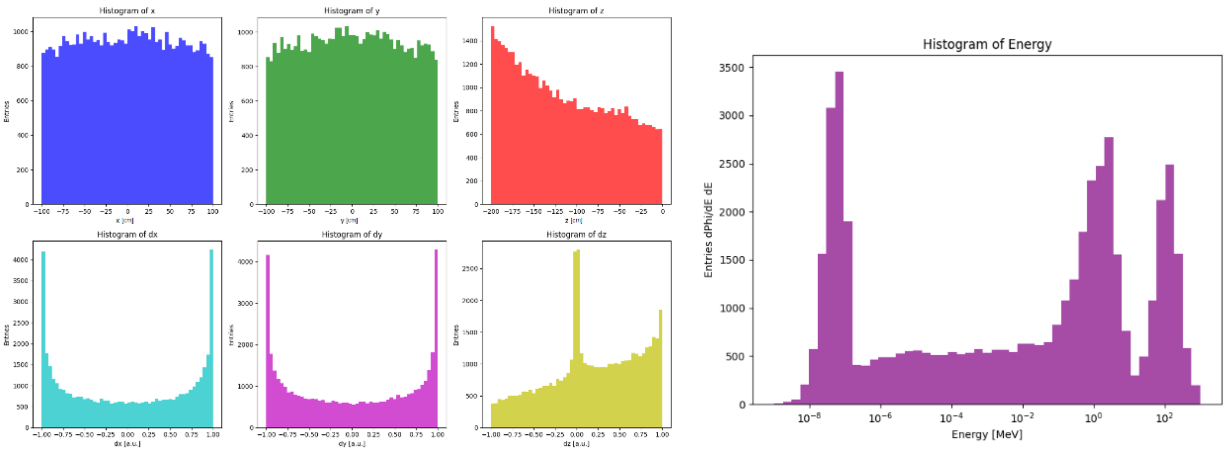

Figure 43. Relative volumetric soil moisture of **100 %**. This represents a theoretical case with no solid domain in the soil so that the whole "soil" volume is composed of water. Histograms of calculated neutron entries with respect to particular axis (left). Neutron energy spectrum (right). Simulation performed with a total of 4.4×10^9 initial neutrons.

7.3 Calculation of CRNS device-specific response to soil moisture using validated Monte Carlo models

The aim of this study is to intercompare the sensitivity of the different CRNS probes under reference conditions that closely resemble real operating conditions. The list of neutrons crossing a 1 m radius virtual sphere around the CRNS detector, provided in the form of a pseudo PTRAC file described in previous sections, was used as the particle source input for subsequent MCNP calculations with the validated models of the different CRNS probes. The Monte Carlo nature of the comparison additionally allows the influence of the measurement geometry to be evaluated, which is particularly relevant for large and asymmetric instruments that can be installed horizontally or vertically and at different heights.

7.3.1 Model of Finapp 3 (Monte Carlo model by CMI)

The validated MCNP model of the Finapp 3 detector (the validation process is described in deliverable D2) was placed at the centre of the virtual sphere described in Section 7.1. The pseudo PTRAC file was processed and used as a source in MCNP simulations of the Finapp 3 response under different volumetric soil moisture conditions, with the following setup:

- Particles originate on the surface of a 1 m radius sphere around the detector.
- Particles from the pseudo PTRAC file are recycled (used multiple times) within a single simulation.

For each soil moisture scenario, the MCNP result was taken as the average of two simulations:

1. Detector located at the sphere centre.
2. Detector located at the sphere centre, rotated by 90 deg around the vertical axis

The response of the Finapp 3 detector in the virtual reference CRNS field was calculated according to the following formula:

$$R = F \cdot C \cdot V \cdot (\frac{n}{N})$$

where:

R is the response, i.e. the total number of detectors counts per one primary neutron in the URANOS calculation of the virtual reference CRNS field.

F is the Finapp 3 MC multiplication factor, *F* = 0.68 ± 10 % (as derived in the Finapp 3 validation work described in deliverable D2).

C is the MCNP result, i.e. the number of neutron interactions per neutron from the pseudo PTRAC file and per 1 cm^3 of scintillator material in the Finapp 3 detector (for a neutron source on a 1 m radius sphere around the detector).

V is the total volume of all scintillator elements in the Finapp 3 detector.

n is the number of neutron entries in the pseudo PTRAC file.

N is the total number of primary neutrons generated in the in URANOS calculation of virtual reference CRNS field.

The results of these calculations for the different volumetric water contents are summarised in Table 4 and shown graphically in Figure 44, with the relative response displayed in Figure 45.

Table 4. Average Finapp 3 detector response and relative response (normalised to 10 % soil moisture) in different soil moisture virtual reference CRNS neutron field. Value of 100 % represents theoretical case with no solid domain in the soil.

Soil moisture [%]	**N [primary neutrons]**	**Average R [counts per primary neutron]**	**u(R) [counts per primary neutron]**	**Relative R (rel. to 10 % soil moisture) [%]**	**u(R) [%]**
1	3.1E+09	3.0E-08	3.0E-09	199 %	2.8
3	3.2E+09	2.2E-08	2.2E-09	144 %	2.8
6	4.0E+09	1.8E-08	1.8E-09	119 %	2.8
10	**1.0E+10**	**1.5E-08**	**1.5E-09**	**100 %**	**2.8**
20	4.0E+09	1.3E-08	1.3E-09	86 %	2.8
30	2.7E+09	1.0E-08	1.1E-09	69 %	2.8
40	4.0E+09	9.9E-09	1.0E-09	66 %	2.8
50	1.0E+10	9.3E-09	9.4E-10	62 %	2.8
100	*4.4E+09*	*6.3E-09*	*6.3E-10*	*42 %*	*2.8*

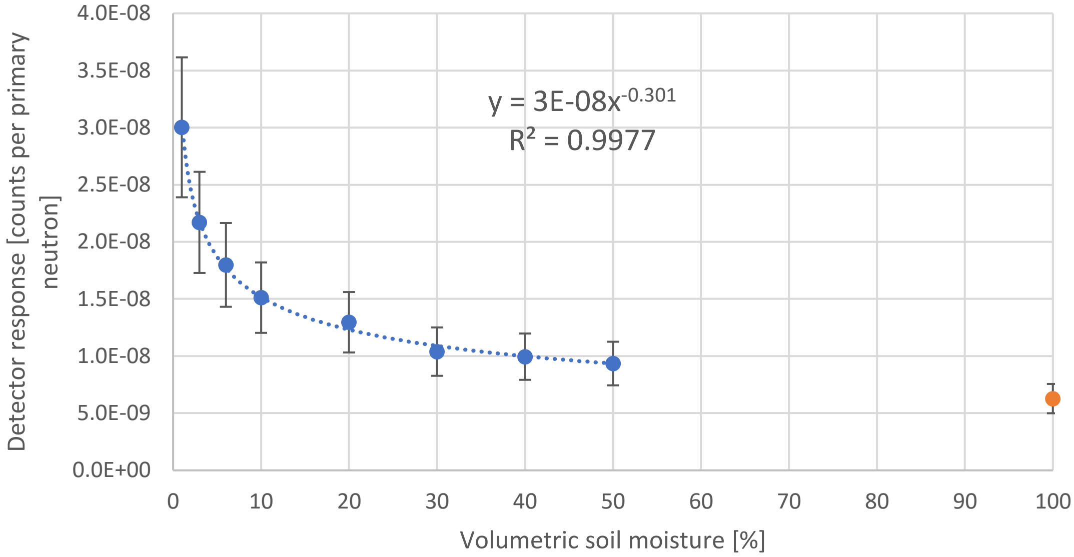

Figure 44. Finapp 3 detector response normalized per one primary neutron (MC model of CMI). Value of 100 % represents a theoretical case with no solid domain in the soil and therefore it is not used for the fit. The error bars correspond to the k = 2, i.e. ~95 % coverage for normal distribution.

The absolute detector response can be well described by a simple two-parameter power law. However, for determining soil moisture in practice, the detector response must be considered *relative* to the reference (field calibration) conditions. The volumetric soil moisture θ can be determined from the relative Finapp 3 detector response using the following equation:

$$\theta = \theta_{cal} \times \left(\frac{N}{N_{cal}}\right)^p = \frac{\theta_{cal}}{N_{cal}^p} \times N^p$$

where:

θ is the volumetric soil moisture,
θ_{cal} is the volumetric soil moisture under calibration conditions,
N is the CRNS count rate (corrected for variations in the incoming neutron flux),
N_{cal} is the CRNS count rate under calibration conditions (also corrected for the incoming neutron flux),
p is the fit parameter; for the Finnap 3 device under the conditions defined in Section 7.1:
***p* = –3.306 ± 2.7 %**

Figure 45 illustrates the practical application of the calculated responses for a detector calibrated at 10 % volumetric soil moisture.

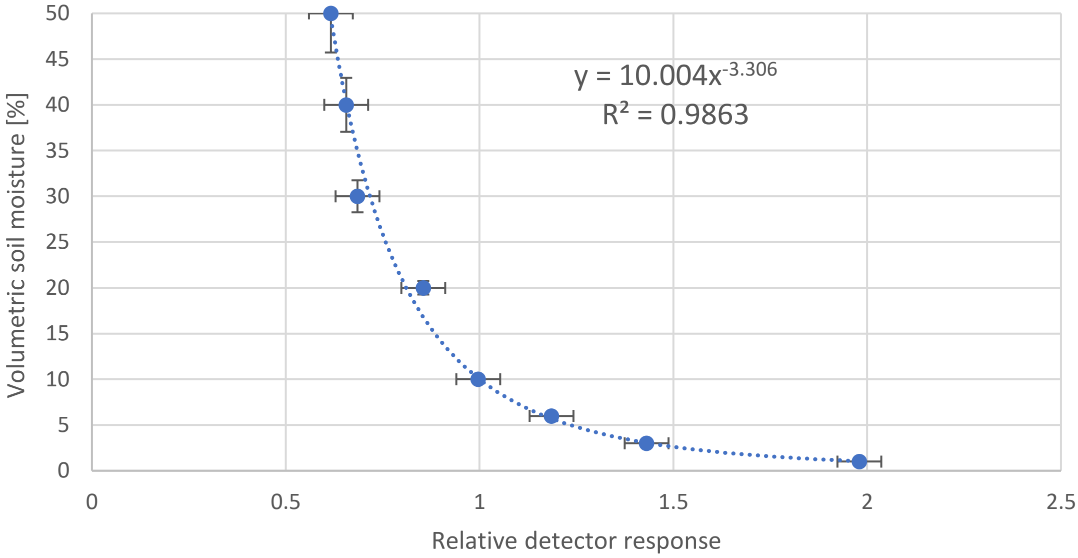

Figure 45. Soil moisture determined from the relative Finapp 3 detector responses (MC model of CMI). The error bars correspond to the k = 2, i.e. ~95 % coverage for normal distribution.

7.3.2 Model of Finapp 3 (Monte Carlo model by SMU)

Because SMU has access only to the executable version of MCNP 6.2, it was not technically possible to process the supplied pseudo PTRAC file directly. Therefore, the validated SMU Finapp 3 model was kindly run by CMI. The response of the Finapp 3 detector in the virtual reference CRNS field was thus calculated in the same way as described in Section 7.3.1, where the response calculation is explained in detail.

The results of the calculations for the different volumetric water contents are summarised in Table 5 and shown in Figure 46. The SMU results are in very good agreement with the CMI results; the multiplication factor F of the SMU Finapp 3 Monte Carlo model is F = 0.78 with a relative uncertainty of 13 %. Figure 47 shows the corresponding inverse relative response curve.

The fitted parameter ***p* = –3.227 ± 2.6 %** agrees with the value obtained for the CMI model within the fit uncertainties.

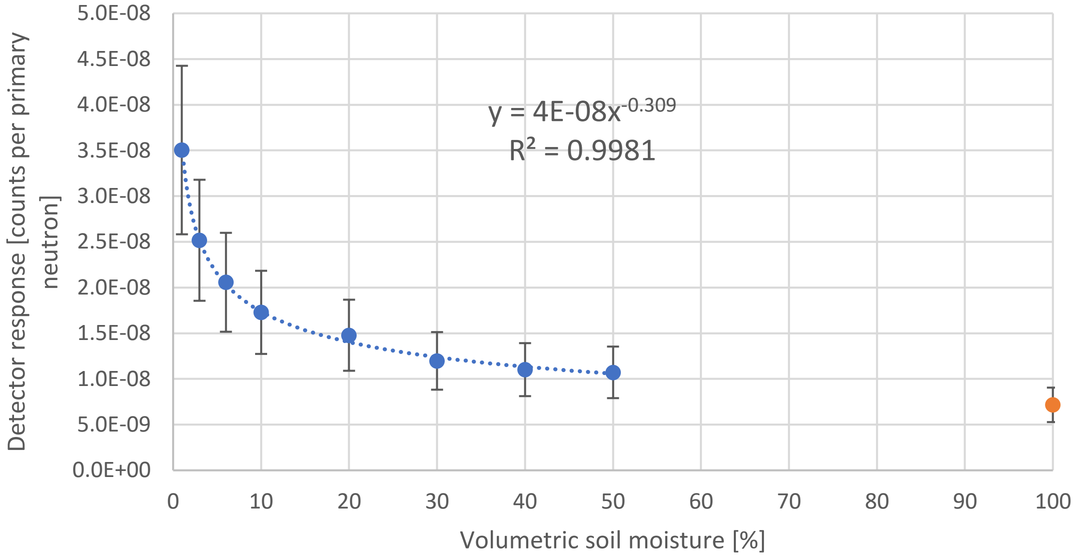

Figure 46. Finapp 3 detector (MC model of SMU) response normalized per one primary neutron. Value of 100 % represents a theoretical case with no solid domain in the soil and therefore it is not used for the fit. The error bars correspond to the k = 2, i.e. ~95 % coverage for normal distribution.

Table 5. SMU Average Finapp 3 detector response and relative response (rel. to 10 % soil moisture) in different soil moisture virtual reference CRNS neutron field. Value of 100 % represents theoretical case with no solid domain in the soil.

Soil moisture [%]	N [primary neutrons]	Average R [counts per primary neutron]	u(R) [counts per primary neutron]	Relative R (rel. to 10 % soil moisture) [%]	u(R) [%]
1	3.1E+09	3.5E-08	4.6E-09	203 %	2.8
3	3.2E+09	2.5E-08	3.3E-09	146 %	2.8
6	4.0E+09	2.1E-08	2.7E-09	119 %	2.8
10	**1.0E+10**	**1.7E-08**	**2.3E-09**	**100 %**	**2.8**
20	4.0E+09	1.5E-08	1.9E-09	86 %	2.8
30	2.7E+09	1.2E-08	1.6E-09	69 %	2.8
40	4.0E+09	1.1E-08	1.4E-09	64 %	2.8
50	1.0E+10	1.1E-08	1.4E-09	62 %	2.8
100	*4.4E+09*	*7.2E-09*	*9.4E-10*	*41 %*	*2.8*

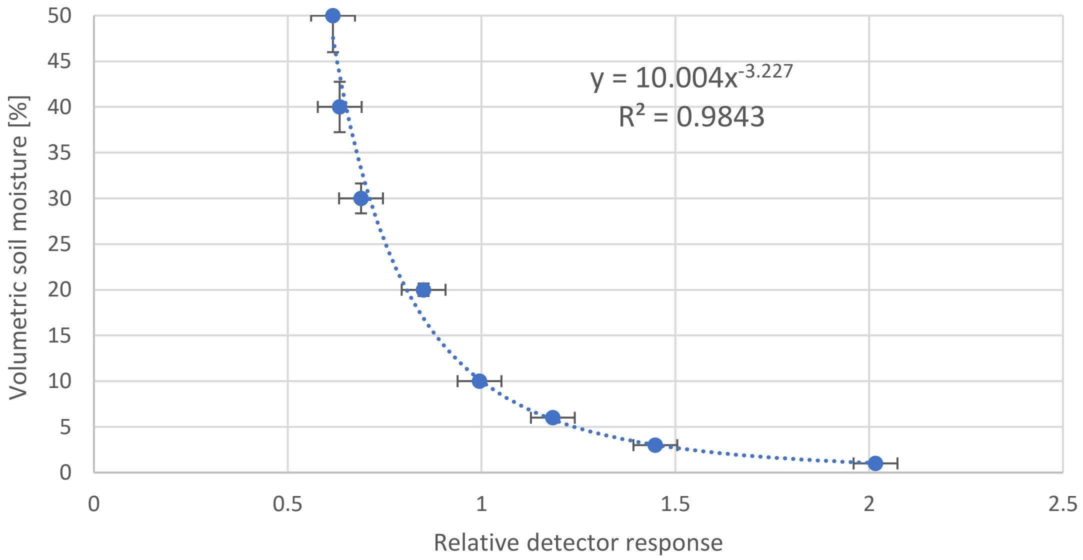

Figure 47. Soil moisture determined from the relative Finapp 3 detector responses (MC model of SMU). The error bars correspond to the k = 2, i.e. ~95 % coverage for normal distribution.

7.3.3 Model of Hydroinnova CRS-1000 He-3 moderated detector

The analysis procedure for the Hydroinnova CRS-1000 He-3 moderated device was analogous to that used for the Finapp 3 detector. The results of the calculations for different volumetric water contents are summarised in Table 6 and shown in Figure 48 and Figure 49.

The fitted parameter is ***p* = –3.154 ± 2.8 %**.

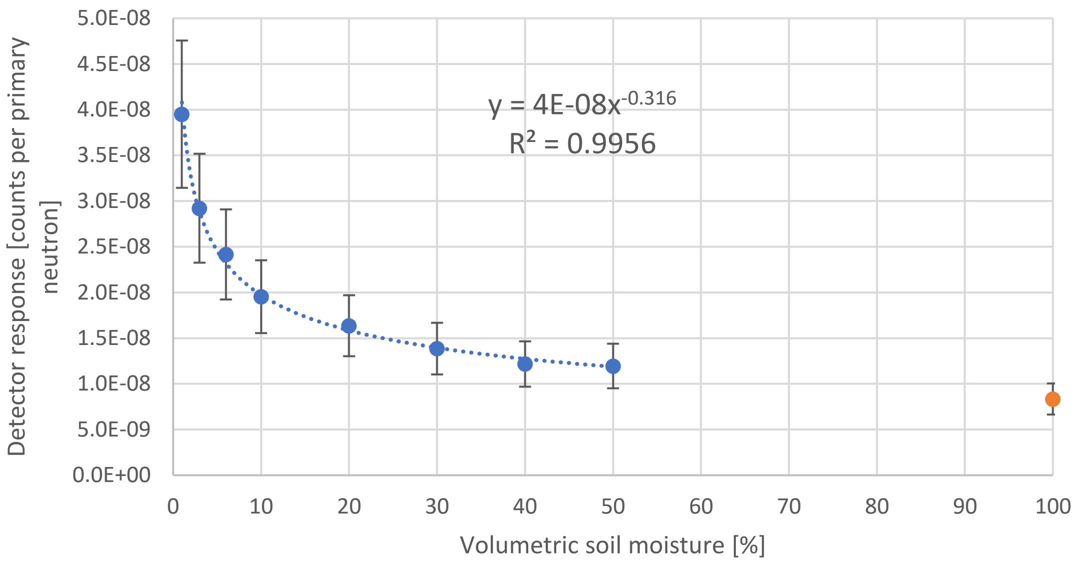

Figure 48. CRS-1000 detector response normalized per one primary neutron. Value of 100 % represents a theoretical case with no solid domain in the soil and therefore it is not used for the fit. The error bars correspond to the k = 2, i.e. ~95 % coverage for normal distribution.

Table 6. Average CRS-1000 detector response and relative response (rel. to 10 % soil moisture) in different soil moisture virtual reference CRNS neutron field. Value of 100 % represents theoretical case with no solid domain in the soil.

Soil moisture [%]	N [primary neutrons]	Average R [counts per primary neutron]	u(R) [counts per primary neutron]	Relative R (rel. to 10 % soil moisture) [%]	u(R) [%]
1	3.1E+09	4.0E-08	4.0E-09	2.02	2.8
3	3.2E+09	2.9E-08	3.0E-09	1.50	2.8
6	4.0E+09	2.4E-08	2.5E-09	1.24	2.8
10	**1.0E+10**	**2.0E-08**	**2.0E-09**	**1.00**	**2.8**
20	4.0E+09	1.6E-08	1.7E-09	0.84	2.8
30	2.7E+09	1.4E-08	1.4E-09	0.71	2.8
40	4.0E+09	1.2E-08	1.2E-09	0.62	2.8
50	1.0E+10	1.2E-08	1.2E-09	0.61	2.8
100	*4.4E+09*	*8.3E-09*	*8.5E-10*	*0.43*	*2.8*

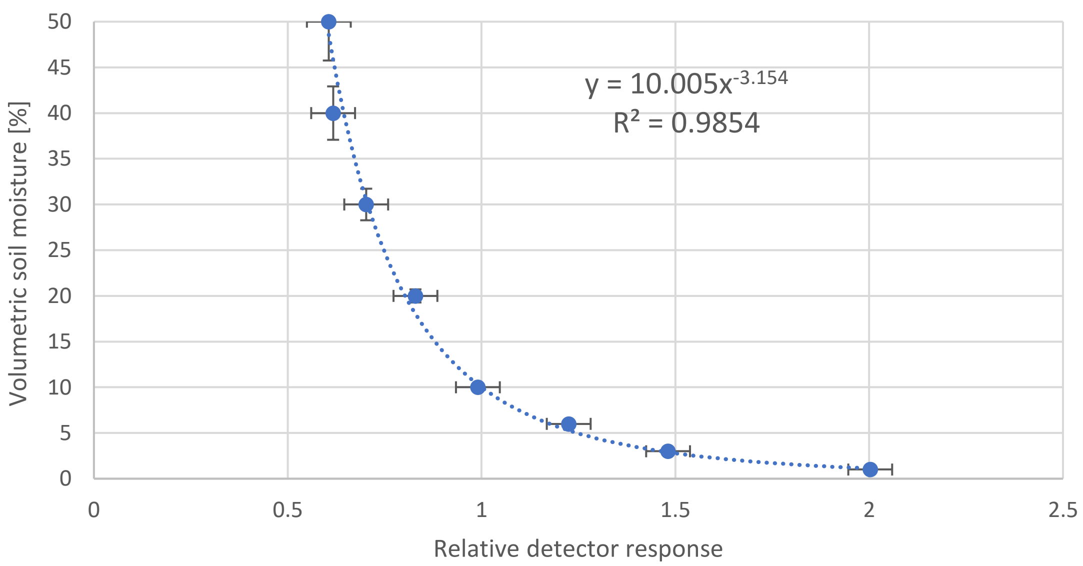

Figure 49. Soil moisture determined from the relative CRS-1000 detector responses. The error bars correspond to the k = 2, i.e. ~95 % coverage for normal distribution.

7.3.4 Model of Hydroinnova CRS-2000/B BF_3 moderated detector

The analysis procedure for the Hydroinnova CRS-2000/B BF_3 moderated device was analogous to that used for the Finapp 3 detector. The results of the calculations for different volumetric water contents are summarised in Table 7 and depicted in Figure 50 and Figure 51.

The fitted parameter is ***p* = –3.209 ± 3.9 %**.

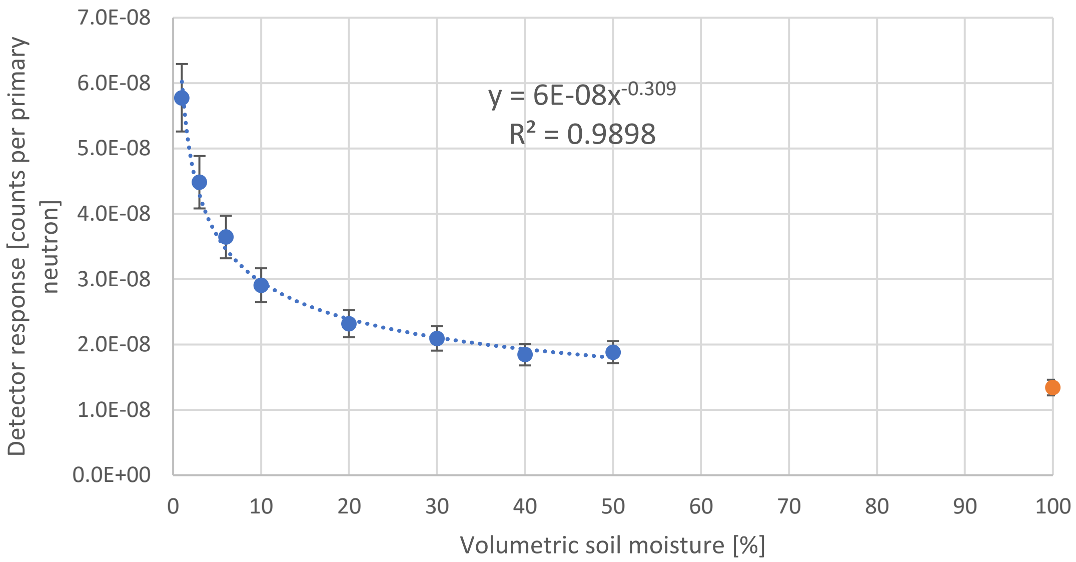

Figure 50. CRS-2000/B detector response normalized per one primary neutron. Value of 100 % represents a theoretical case with no solid domain in the soil and therefore it is not used for the fit. The error bars correspond to the k = 2, i.e. ~95 % coverage for normal distribution.

Table 7. Average CRS-2000/B detector response and relative response (rel. to 10 % soil moisture) in different soil moisture virtual reference CRNS neutron field. Value of 100 % represents a theoretical case with no solid domain in the soil.

Soil moisture [%]	N [primary neutrons]	Average R [counts per primary neutron]	u(R) [counts per primary neutron]	Relative R (rel. to 10 % soil moisture) [%]	u(R) [%]
1	3.1E+09	5.8E-08	2.6E-09	1.99	2.8
3	3.2E+09	4.5E-08	2.0E-09	1.54	2.8
6	4.0E+09	3.6E-08	1.6E-09	1.25	2.8
10	**1.0E+10**	**2.9E-08**	**1.3E-09**	**1.00**	**2.8**
20	4.0E+09	2.3E-08	1.0E-09	0.80	2.8
30	2.7E+09	2.1E-08	9.4E-10	0.72	2.8
40	4.0E+09	1.8E-08	8.2E-10	0.63	2.8
50	1.0E+10	1.9E-08	8.4E-10	0.65	2.8
100	*4.4E+09*	*1.3E-08*	*6.0E-10*	*0.46*	*2.8*

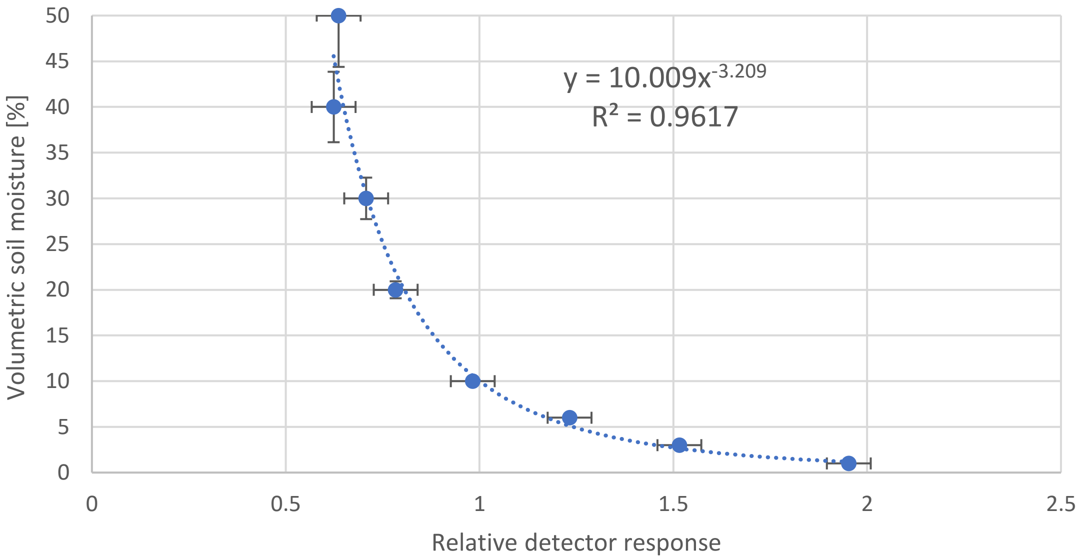

Figure 51. Soil moisture determined from the relative CRS-2000/B detector responses. The error bars correspond to the k = 2, i.e. ~95 % coverage for normal distribution.

7.3.5 Model of StyX Neutronica System S1

The analysis procedure for the StyX Neutronica System S1 device was analogous to that used for the Finapp 3 detector. The results of the calculations for different volumetric water contents are summarised in Table 8 and shown in Figure 52 and Figure 53.

Figure 52 presents the System S1 detector response normalised per one primary neutron. The value at 100 % volumetric water content represents a theoretical case with no solid phase in the soil domain and is therefore not used in the fit. The error bars correspond to $k = 2$, i.e. approximately 95 % coverage for a normal distribution.

The fitted parameter is ***p* = –2.983 ± 2.6 %**.

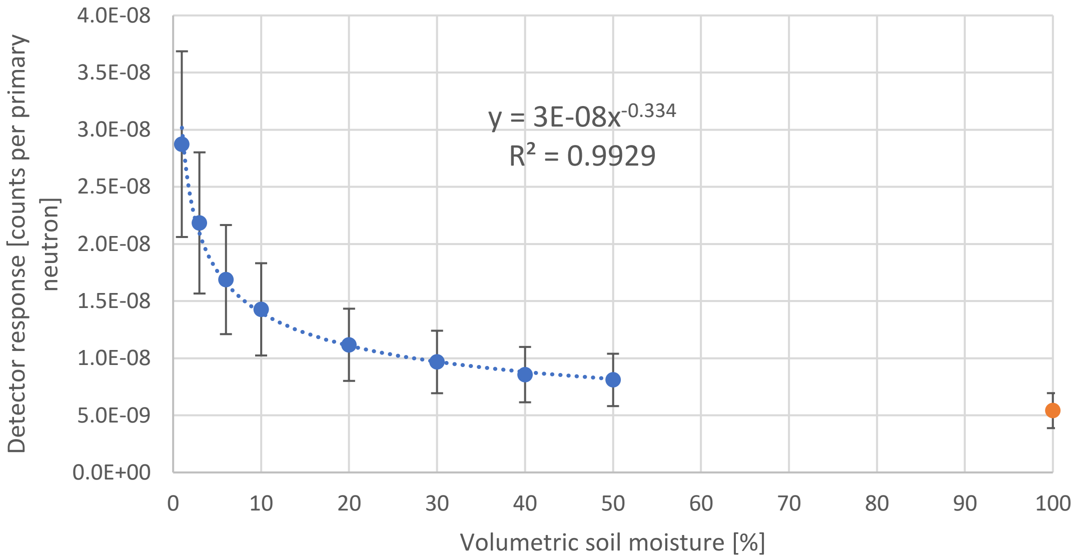

Figure 52. System S1 detector response normalized per one primary neutron. Value of 100 % represents a theoretical case with no solid domain in the soil and therefore it is not used for the fit. The error bars correspond to the k = 2, i.e. ~95 % coverage for normal distribution.

Table 8. Average StyX System S1 detector response and relative response (rel. to 10 % soil moisture) in different soil moisture virtual reference CRNS neutron field. Value of 100 % represents a theoretical case with no solid domain in the soil.

Soil moisture [%]	N [primary neutrons]	Average R [counts per primary neutron]	u(R) [counts per primary neutron]	Relative R (rel. to 10 % soil moisture) [%]	u(R) [%]
1	3.1E+09	2.9E-08	8.1E-09	2.01	2.8
3	3.2E+09	2.2E-08	6.2E-09	1.53	2.8
6	4.0E+09	1.7E-08	4.8E-09	1.18	2.8
10	**1.0E+10**	**1.4E-08**	**4.0E-09**	**1.00**	**2.8**
20	4.0E+09	1.1E-08	3.2E-09	0.78	2.8
30	2.7E+09	9.7E-09	2.7E-09	0.68	2.8
40	4.0E+09	8.6E-09	2.4E-09	0.60	2.8
50	1.0E+10	8.1E-09	2.3E-09	0.57	2.8
100	*4.4E+09*	*5.4E-09*	*1.5E-09*	*0.38*	*2.8*

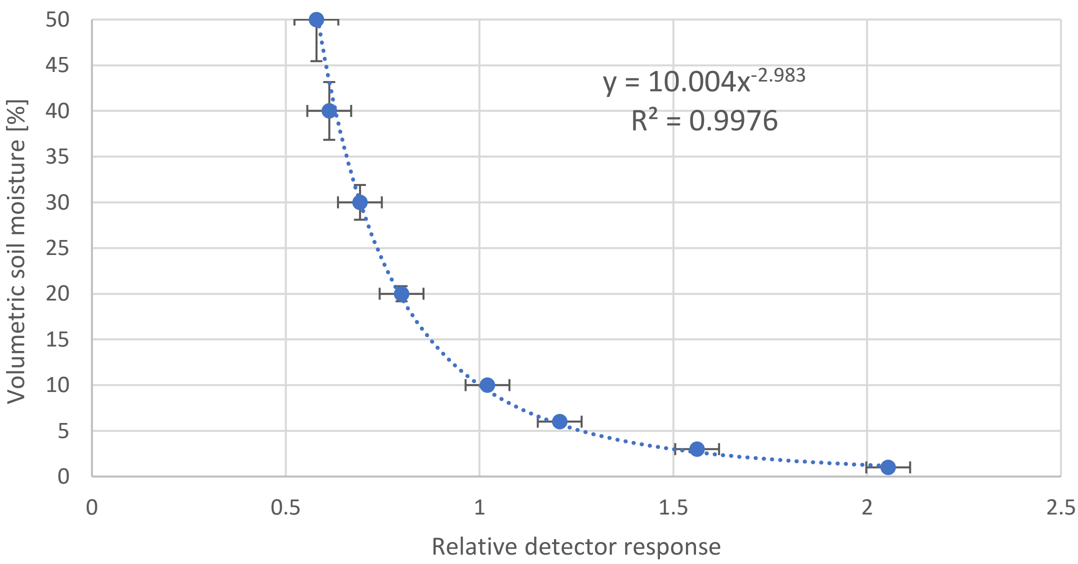

Figure 53. Soil moisture determined from the relative System S1 detector responses. The error bars correspond to the k = 2, i.e. ~95 % coverage for normal distribution.

8 Model-based conversion of CRNS neutron response to volumetric soil moisture: evaluation of conversion functions

At present, several different models are used within the CRNS community to derive soil moisture from CRNS probe count rates. In this work, predictions from the validated Monte Carlo-based models of the CRNS probes were compared with the following two approaches:

- the **N0 equation** from the publication Desilets et al. (2010), using the commonly adopted parameter set (0.0808, 0.372, 0.115), recalculated to volumetric soil moisture, inverted and scaled relatively to 10 % soil moisture

- the **Universal Transport Solution (UTS) equation** from the publication Köhli et al. (2021) using the parameter set “MCNP drf (full)” for an air humidity of 10 g/m^3, likewise scaled to 10 % soil moisture

The results are summarised in Figure 54. It is evident that the Monte Carlo-based predictions for all characterised CRNS probes agree more closely with the newer UTS model over the full range of volumetric soil moisture. The N0 model may perform satisfactorily, but typically only over a limited soil moisture interval that depends on the parameter choices.

However, in practice we need to derive soil moisture from the neutron count rate detected by a CRNS probe, and for this we require the inverse relationship. This is rather difficult to obtain for the complex, multi-parameter UTS model. It was found that the Monte Carlo-based model behaviour under different soil moisture conditions can be well described by a power function. The inverse relationship is therefore also a power function, which makes the analysis much simpler. The corresponding inverse functions to those shown in Figure 54 are presented in Figure 55.

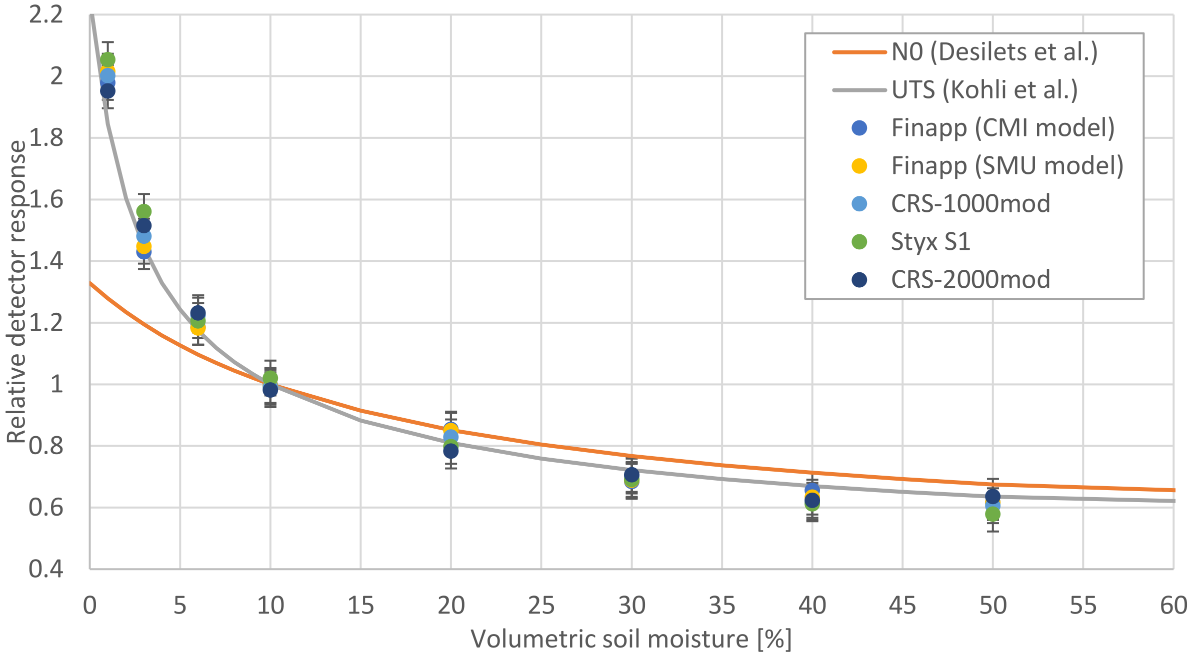

Figure 54. Relative detector response, as derived from the MCNP-based characterisation of the individual CRNS devices in this deliverable, as a function of volumetric soil moisture. The two currently used models, N0 and UTS, are compared in terms of how well they describe this soil-moisture–CRNS-response relationship. The error bars correspond to the k = 2, i.e. ~95 % coverage for normal distribution.

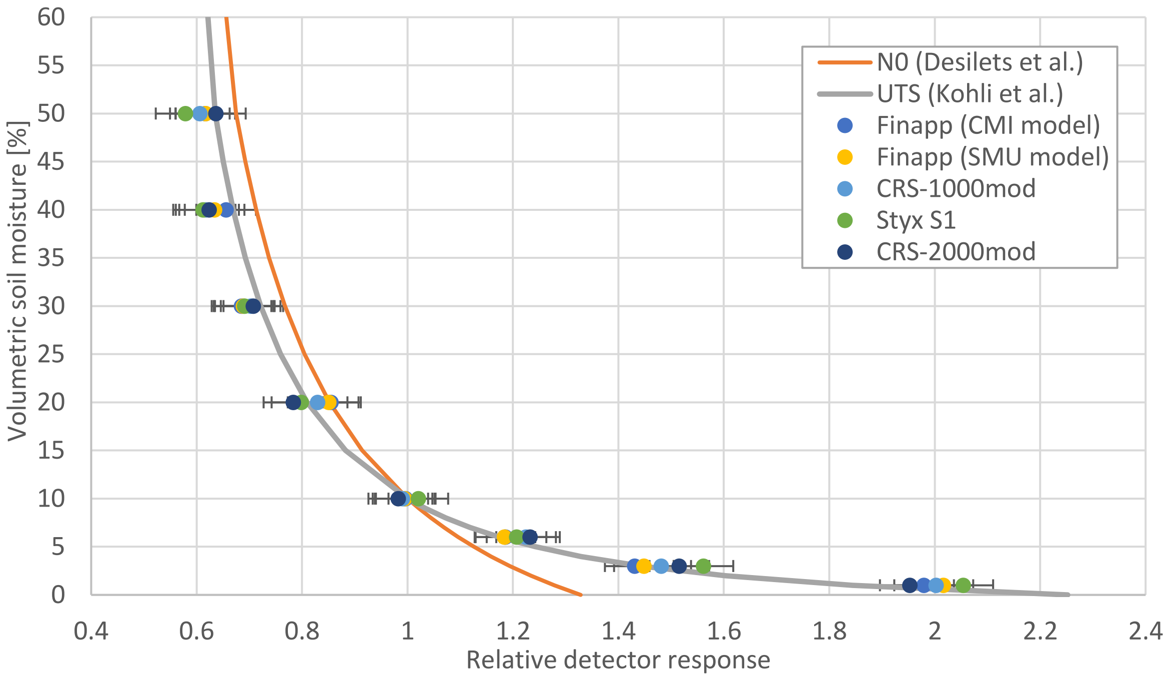

Figure 55. Soil moisture determined from the relative detector responses of different CRNS systems, based on inverse functions to those shown in Figure 54. The two currently used models, N0 and UTS, are compared in terms of how well they describe this CRNS-response–soil-moisture relationship. The error bars correspond to the k = 2, i.e. ~95 % coverage for normal distribution.

The analysis shows that the different devices behave similarly under the reference conditions, and that the relative volumetric soil moisture θ can be determined from the relative detector response using the following equation:

$$\theta = \theta_{cal} \times \left(\frac{N}{N_{cal}}\right)^{p} = \frac{\theta_{cal}}{N_{cal}^{p}} \times N^{p}$$

where:
θ is the volumetric soil moisture,
θ_{cal} is the volumetric soil moisture under calibration conditions,
N is the CRNS count rate (corrected for variations in the incoming neutron flux),
N_{cal} is the CRNS count rate under calibration conditions (also corrected for incoming neutron flux),
p is the fit parameter specific to the particular CRSN device operating above soil composition described in Section 7.1.

The values of fitted parameter *p* for the different instruments are summarised in Table 9.

Table 9. Summary of the determined fit parameters ***p*** to be used for the in-field volumetric soil moisture determination.

Manufacturer	CRNS model	MC model author	Soil type (assumed in all cases)	Fit parameter *p*
Finapp	Finapp Model 3	CMI, SMU	75 $\%_{Vol}$ SiO_2 25 $\%_{Vol}$ Al_2O_3 compound density of 2.86 g/cm^3	-3.267 ± 2.6 %*
Hydroinnova	CRS-1000 mod	PTB		-3.154 ± 2.8 %
Hydroinnova	CRS-2000/B mod	CIEMAT		-3.209 ± 3.9 %
StyX Neutronica	System S1	PTB		-2.983 ± 2.6 %

*Average from the two different models

9 Conclusions

The project SoMMet aimed to harmonise soil moisture measurements across multiple scales and to provide a more consistent basis for the determination of environmental soil water content. The CRNS methodology sits at the intermediate scale between remote sensing and point-scale sensors and is the focus of this deliverable.

This deliverable built upon deliverable D2, where the most common state-of-the-art CRNS probes, currently used in existing CRNS networks worldwide, were selected and their virtual models were developed within the MCNP Monte Carlo transport code. Furthermore, these digital twins for CRNS detectors were validated in systematic irradiation campaigns in neutron metrology laboratories using “artificial” neutrons from well-characterised reference fields.

In this deliverable D3, the CRNS method was “taken from the laboratory to the outdoor world”. Time series were recorded with the CRNS systems at the three SoMMet test field sites of Bondeno, Foggia and Marquardt and were analysed to investigate the performance and systematic effects of the instruments under outdoor conditions. The total neutron fluence rate was determined by the SI-traceable extended-range Bonner Sphere Spectrometers (ERBSS), capable of detecting neutron radiation across roughly 12 orders of magnitude in energy (from about 10^{-8} MeV up to about 10^{4} MeV). In parallel, a reduced version of this spectrometer, the W-PIE, and a mobile CRNS rover were deployed at the SoMMet sites. These instruments provided reference and additional datasets on neutron count rates and neutron energy distributions. The combined measurements yielded a holistic dataset for the interpretation of CRNS signals and the validation of transport models.

With the neutron transport code URANOS, detailed digital twins of the three SoMMet sites were developed. The voxel-based models relied on site-specific information on soil bulk density and moisture profiles, biomass water equivalent, vegetation structure, land use and topography. URANOS simulations were then used to characterise the CRNS footprint and depth sensitivity, the influence of vegetation and other hydrogen pools, and the response of CRNS to changing soil moisture. The simulated neutron spectra and the derived count rates were benchmarked against Bonner-sphere-unfolded spectra and measured CRNS time series (in several cases also under dynamic soil moisture conditions). The comparisons showed good agreement in the energy ranges most relevant for CRNS and allowed the main sources of uncertainty to be quantified. This benchmarking gave additional confidence in using URANOS to study and characterise CRNS performance.

Furthermore, an intercomparison study of the selected CRNS detector types was carried out. Because the actual operating conditions in the field have more complex neutron energy and angular distributions compared with those in laboratory reference fields, a novel concept, the “virtual reference CRNS neutron field”, was developed. This concept made it possible to test and compare different CRNS systems virtually under well-defined and harmonised conditions that realistically modelled their operating environment. The intercomparison was implemented through dedicated Monte Carlo–based simulations, in which the laboratory-validated CRNS digital twin models were coupled with the URANOS-based virtual environment. By scaling environmental and meteorological parameters, with soil moisture being one of the most important in this study, their neutron response to soil moisture conditions was analysed in detail. This approach made it possible to establish a sound link between soil moisture and the neutron fluence rate reaching a virtual neutron detector situated above ground. In future, this method could also be extended to airborne sensors.

For end users, the outcome of this work is an improved quantitative understanding of the neutron response of CRNS systems and its dependence on soil moisture. By inverting the modelled neutron response–soil moisture relationship, it becomes possible to derive soil moisture from observed CRNS count rates on a physically validated basis. Finally, methods for converting CRNS response to volumetric soil moisture were evaluated using the results from the simulation chain up to the virtual reference CRNS neutron field concept. It was demonstrated that the Universal Transport Solution (UTS) equation successfully describes the conversion from neutron response to soil moisture for the four different CRNS device types and across a wide range of volumetric soil moisture values. Overall, these results represent a significant advancement of the CRNS methodology. It is expected that they will support its wider uptake by end users in applications in agriculture, hydrology, climate science and, in particular, they will support the calibration/validation efforts in the remote sensing community.

It should be noted that, despite these novel results that will advance the CRNS methodology, on-field calibration of CRNS sensors cannot be omitted. In practice, a site-specific relationship is still required between the CRNS neutron count rate (representing the integral soil moisture) and local soil moisture information obtained, for example, from manual soil sampling and gravimetric analysis. The topic of on-field calibration practices for CRNS sensors is addressed in more detail in SoMMet deliverable D4. It is expected that, in the near future, the URANOS-based simulation framework and the results reported in this deliverable D3 will support community efforts to make on-field calibration more efficient and harmonised.

10 References

Agostinelli, S., Allison, J., Amako, K., Apostolakis, J., Araujo, H., Arce, P., ... Yoshida, H. (2003). GEANT4 – a simulation toolkit. *Nuclear Instruments and Methods in Physics Research Section A: Accelerators, Spectrometers, Detectors and Associated Equipment, 506*(3), 250–303. https://doi.org/10.1016/S0168-9002(03)01368-8

Andreasen, M., Jensen, K. H., Desilets, D., Franz, T. E., Zreda, M., Bogena, H. R., & Looms, M. C. (2017). Status and perspectives on the cosmic-ray neutron method for soil moisture estimation and other environmental science applications. *Vadose Zone Journal, 16*(8). https://doi.org/10.2136/vzj2017.04.0086

Birattari, C., Cappellaro, P., Mitaroff, A., & Silari, M. (2001). Development of an extended range Bonner sphere spectrometer. In *Advanced Monte Carlo for Radiation Physics, Particle Transport Simulation and Applications* (pp. 1157–1162). Springer. https://doi.org/10.1007/978-3-642-18211-2_185

Bogena, H. R., Schrön, M., Jakobi, J., Ney, P., Zacharias, S., & Vereecken, H. (2022). COSMOS-Europe: A European network of cosmic-ray neutron soil moisture sensors. *Earth System Science Data, 14*(3), 1125–1151. https://doi.org/10.5194/essd-14-1125-2022

Bramblett, R. L., Ewing, R. I., & Bonner, T. W. (1960). A new type of neutron spectrometer. *Nuclear Instruments and Methods, 9*(1), 1–12. https://doi.org/10.1016/0029-554X(60)90043-4

Cheminet, A., Lacoste, V., Gressier, V., Hubert, G., Martin, A., & Pépino, M. (2012). Characterization of the IRSN neutron multisphere spectrometer (HERMEIS) at European standard calibration fields. *Journal of Instrumentation, 7*(04), C04007–C04007. https://doi.org/10.1088/1748-0221/7/04/C04007

Cirillo, A., Meucci, R., Caresana, M., & Caresana, M. (2021). An innovative neutron spectrometer for soil moisture measurements. *The European Physical Journal Plus, 136*(10), 985. https://doi.org/10.1140/epjp/s13360-021-01976-x

Clem, J. M., & Dorman, L. I. (2000). Neutron monitor response functions. *Space Science Reviews, 93*(1–2), 335–359. https://doi.org/10.1023/A:1026508915269

Desilets, D., Zreda, M., & Ferré, T. P. A. (2010). Nature's neutron probe: Land surface hydrology at an elusive scale with cosmic rays. *Water Resources Research, 46*(11), W11505. https://doi.org/10.1029/2009WR008726

Gianessi, S., Polo, M., Stevanato, L., Lunardon, M., Ahmed, H. S., Weltin, G., ... Baroni, G. (2021). Assessment of a new non-invasive soil moisture sensor based on cosmic-ray neutrons. In *2021 IEEE International Workshop on Metrology for Agriculture and Forestry (MetroAgriFor)* (pp. 290–294). IEEE. https://doi.org/10.1109/metroagrifor52389.2021.9628451

Goorley, T., James, M., Booth, T., Brown, F., Bull, J., Cox, L. J., ... Zukaitis, T. (2012). Initial MCNP6 release overview. *Nuclear Technology, 180*(3), 298–315. https://doi.org/10.13182/NT11-135

Köhli, M., Schrön, M., Zreda, M., Schmidt, U., Dietrich, P., & Zacharias, S. (2015). Footprint characteristics revised for field-scale soil moisture monitoring with cosmic-ray neutrons. *Water Resources Research, 51*(7), 5772–5790. https://doi.org/10.1002/2015WR017169

Köhli, M., Weimar, J., Schrön, M., Budach, C., & Schmidt, U. (2018). Response functions for detectors in cosmic ray neutron sensing. *Nuclear Instruments and Methods in Physics Research Section A: Accelerators, Spectrometers, Detectors and Associated Equipment, 902*, 184–189. https://doi.org/10.1016/j.nima.2018.06.052

Köhli, M., Weimar, J., Schrön, M., Baatz, R., & Schmidt, U. (2021). Soil moisture and air humidity dependence of the above-ground cosmic-ray neutron intensity. *Frontiers in Water, 2*, 544847. https://doi.org/10.3389/frwa.2020.544847

Köhli, M., Schrön, M., Zacharias, S., & Schmidt, U. (2023). URANOS v1.0 – the Ultra Rapid Adaptable Neutron-Only Simulation for environmental research. *Geoscientific Model Development, 16*(2), 449–477. https://doi.org/10.5194/gmd-16-449-2023

Köhli, M., Schrön, M., Zacharias, S., & Schmidt, U. (2025). URANOS – a novel voxel engine neutron transport Monte-Carlo simulation. *Journal of Physics: Conference Series, 3130*(1), 012017. https://doi.org/10.1088/1742-6596/3130/1/012017

Neumaier, S., Arnold, D., Böhm, J., & Funck, E. (2000). The PTB underground laboratory for dosimetry and spectrometry. *Applied Radiation and Isotopes, 53*(1–2), 173–178. https://doi.org/10.1016/S0969-8043(00)00129-9

Reginatto, M., Goldhagen, P., & Neumann, S. (2002). Spectrum unfolding, sensitivity analysis and propagation of uncertainties with the maximum entropy deconvolution code MAXED. *Nuclear Instruments and Methods in Physics Research Section A: Accelerators, Spectrometers, Detectors and Associated Equipment, 476*(1–2), 242–246. https://doi.org/10.1016/S0168-9002(01)01439-5

Sato, T., & Niita, K. (2006). Analytical Functions to Predict Cosmic-Ray Neutron Spectra in the Atmosphere. *Radiat. Res.* 166, 544–555 (2006). https://doi.org/10.1667/RR0610.1

Sato, T., Niita, K., Matsuda, N., Hashimoto, S., Iwamoto, Y., Furuta, T., ... Sihver, L. (2015). Overview of particle and heavy ion transport code system PHITS. *Annals of Nuclear Energy, 82*, 110–115. https://doi.org/10.1016/j.anucene.2014.08.023

Sato, T. (2016). Analytical model for estimating the zenith angle dependence of terrestrial cosmic ray fluxes. *PLOS ONE, 11*(8), e0160390. https://doi.org/10.1371/journal.pone.0160390

Schrön, M., Rosolem, R., Köhli, M., Piussi, L., Schröter, I., Iwema, J., ... Zacharias, S. (2018). Cosmic-ray neutron rover surveys of field soil moisture and the influence of roads. *Water Resources Research, 54*(9), 6441–6459. https://doi.org/10.1029/2017WR021719

Thomas, D., Alevra, A. V. (2002). Bonner sphere spectrometers—a critical review. *Nuclear Instruments and Methods in Physics Research Section A: Accelerators, Spectrometers, Detectors and Associated Equipment, 476*(1–2), 12–20. https://doi.org/10.1016/S0168-9002(01)01379-1

Weimar, J., Köhli, M., Budach, C., & Schmidt, U. (2020). Large-scale boron-lined neutron detection systems as a ^{3}He alternative for cosmic ray neutron sensing. *Frontiers in Water, 2*, 16. https://doi.org/10.3389/frwa.2020.00016

Wiegel, B., & Alevra, A. V. (2002). NEMUS – the PTB neutron multisphere spectrometer: Bonner spheres and more. *Nuclear Instruments and Methods in Physics Research Section A: Accelerators, Spectrometers, Detectors and Associated Equipment, 476*(1–2), 36–41. https://doi.org/10.1016/S0168-9002(01)01385-7

Ziegler, J. F. (1996). Terrestrial cosmic rays. *IBM Journal of Research and Development, 40*(1), 19–39. https://doi.org/10.1147/rd.401.0019

Zreda, M., Desilets, D., Ferré, T. P. A., & Scott, R. L. (2008). Measuring soil moisture content non-invasively at intermediate spatial scale using cosmic-ray neutrons. *Geophysical Research Letters, 35*(21), L21402. https://doi.org/10.1029/2008GL035655

Zreda, M., Shuttleworth, W. J., Zeng, X., Zweck, C., Desilets, D., Franz, T., & Rosolem, R. (2012). COSMOS: The COsmic-ray Soil Moisture Observing System. *Hydrology and Earth System Sciences, 16*(11), 4079–4099. https://doi.org/10.5194/hess-16-4079-2012

Appendix A: Examples of greyscale input matrices for URANOS representation of SoMMet sites

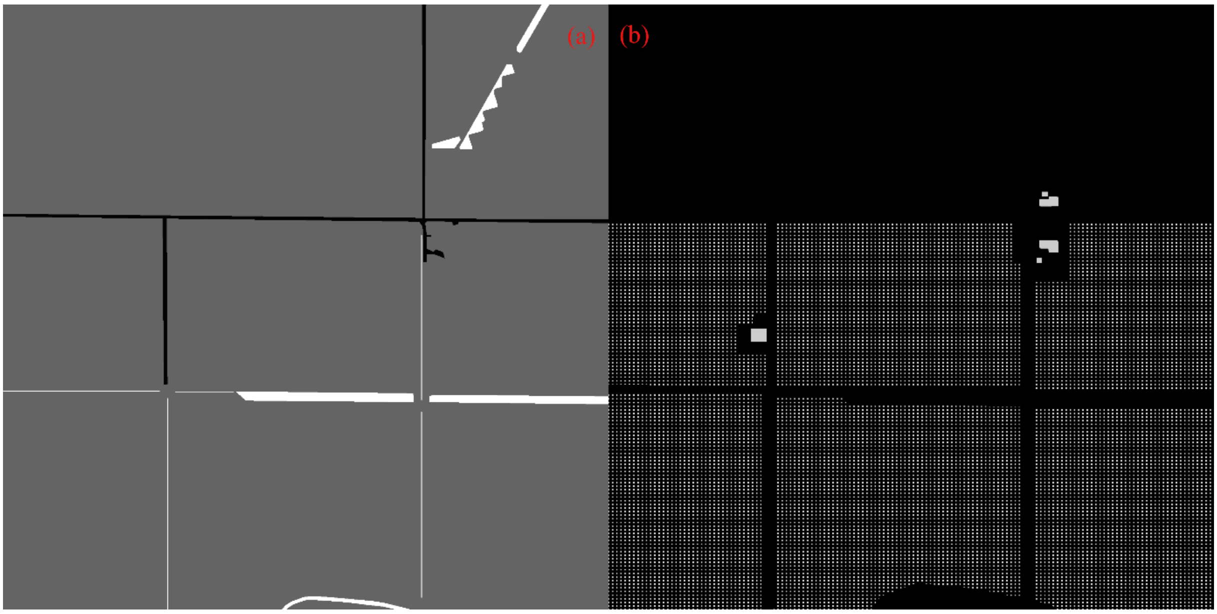

Figure A 1. Greyscale input matrix examples (grey values in brackets) for the URANOS representation of the Bondeno high-level site. (a) Uppermost ground layer showing soil in grey (100), dry dirt roads in black (6) and water ponds and a river in white (254). (b) Canopy layer 2.5–4 m above the soil consisting of air in black (1), buildings in grey (203) and low-density tree canopy in light grey (221).

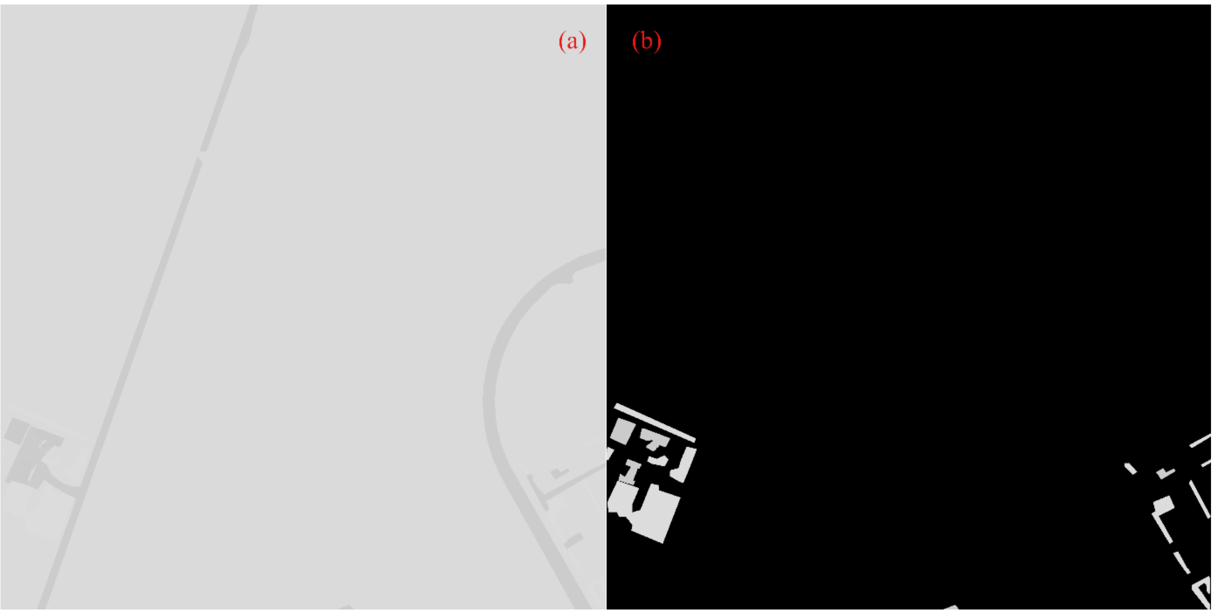

Figure A 2. Greyscale input matrix examples (grey values in brackets) for the URANOS representation of the Foggia high-level site. (a) Grass in light grey (218) on top of the soil, with street/concrete structures in darker grey (204). (b) Building and tree layer from 2.5 to 5 m height, composed of air in black (1), buildings in grey (203) and trees in light grey (220).

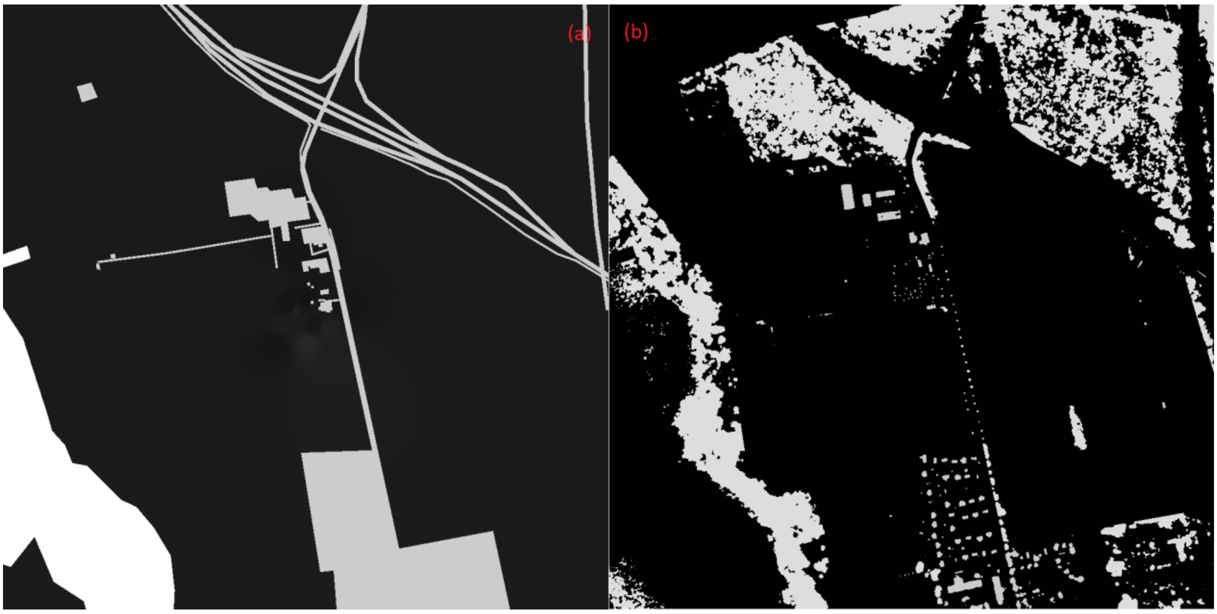

Figure A 3. Caption Greyscale input matrix examples (grey values in brackets) for the URANOS representation of the Marquardt high-level site. (a) Uppermost soil layer (first cm) containing a water pool in white (254, lower left), concrete below a nearby settlement, streets and buildings in grey (204), and a resolved soil moisture map with values mostly between 20 and 40 (corresponding to 10–20 Vol-%). (b) Building and tree layer from 4.5 to 5 m height, composed of air in black (1), buildings in grey (203) and trees in light grey (220/221).